

**AN ADAPTIVE BATTERY ENERGY STORAGE SYSTEM
CONTROLLER FOR ENHANCING FREQUENCY
STABILITY OF A LOW INERTIA GRID**

A thesis submitted to
the Department of Electrical and Electronic Engineering
of
Bangladesh University of Engineering and Technology
in partial fulfillment of the requirements
for the degree of
Master of Science in
Electrical and Electronic Engineering
by

Md. Mahadi Hasan: 1018062130



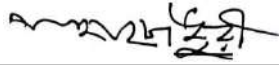
Department of Electrical and Electronic Engineering
BANGLADESH UNIVERSITY OF ENGINEERING AND TECHNOLOGY

25 July, 2023

APPROVAL CERTIFICATE

The thesis titled “An adaptive battery energy storage system controller for enhancing frequency stability of a low inertia grid” submitted by Md. Mahadi Hasan, Roll No.: 1018062130, Session: October 2018, has been accepted as satisfactory in partial fulfillment of the requirement for the degree of Master of Science in Electrical and Electronic Engineering on 25/07/2023.

BOARD OF EXAMINERS



1. Dr. Abdul Hasib Chowdhury
Professor
Department of EEE, BUET, Dhaka

Chairman
(Supervisor)



2. Dr. Md. Aynal Haque
Professor & Head
Department of EEE, BUET, Dhaka

Member
(Ex-Officio)



3. Dr. Mohammad Jahangir Alam
Professor
Department of EEE, BUET, Dhaka

Member



4. Dr. Md. Ziaur Rahman Khan
Professor
Department of EEE, BUET, Dhaka

Member



5. Dr. Md. Minarul Islam
Assistant Professor
Department of EEE, University of Dhaka, Dhaka

Member
(External)

CANDIDATE'S DECLARATION

This is to certify that the work entitled “**An adaptive battery energy storage system controller for enhancing frequency stability of a low inertia grid**” is the outcome of research carried out by me under the supervision of Dr. Abdul Hasib Chowdhury. It is hereby declared that this thesis/project or any part of it has not been submitted elsewhere for the award of any degree or diploma.



Md. Mahadi Hasan

Student ID:

1018062130

DEDICATION

To my dearest Parents

TABLE OF CONTENTS

Declaration	...iii
Table of Contents	...v
List of Figures	...vii
List of Tables	...xi
List of Abbreviations of Technical Symbols and Terms	...xii
Acknowledgements	...xiii
Abstract	...xiv
Chapter-1: Introduction	01
1.1 Motivation	01
1.2 Objectives	02
1.3 Methodology	03
1.4 Thesis Outline	03
Chapter-2: Literature Review	05
2.1 Renewable Energy	05
2.2 Low Inertia Grid and System Stability	07
2.3 Inverter Control and Virtual Inertia Emulation	08
2.3.1 Grid Forming Inverter	09
2.3.2 Grid Feeding Inverter	11
2.3.3 Grid Supporting Inverter	12
2.3.4 Virtual Inertia Emulation Techniques	12
2.4 BESS Applications for Inertial Improvement	18
Chapter-3: DQ0 Algorithm Based Inverter Control	22
3.1 DQ0 Transformation and Inverter Controller	22
3.2 Simulation Setup	24
3.3 Case Study and Simulation Results	27
3.3.1 Case study-1: Constant Irradiance and Varying Loads	27
3.3.2 Case study-2: Dynamic Weather Condition and Constant Load	28

3.3.3 Case study-3: Three Phase Fault at Point of Common Coupling	31
3.3.4 Case study-4: Three Phase Short Circuit Fault at the Inverter Side	32
3.3.5 Case study-5: Short Circuit Fault on the DC Link Capacitor Side	34
3.3.5.1 Fault Applied for 0.05 Seconds (from 0.30 s to 0.35 s)	34
3.3.5.2 Fault Applied for 0.02 Seconds (from 0.30 s to 0.32 s)	35
3.4 Discussion	37
Chapter-4: Adaptive Battery Energy Storage System Controller Design	38
4.1 Proposed Adaptive Fuzzy-ANFIS Hybrid Controller	38
4.1.1 Fuzzy logic Inference System Design	39
4.1.2 Adaptive Neuro-Fuzzy Inference System (ANFIS) Design	42
4.2 Components Model and Specifications	44
4.2.1 Battery Energy Storage System (BESS)	44
4.2.2 Bi-directional Converter and Inverter	46
4.3 Software Implementation	48
Chapter-5: Simulation Results and Discussions	51
5.1 Case Study Sequence	51
5.2 With a BESS Utilizing FLC and PI Controller	52
5.2.1 Sudden Load Variations (i.e. Load Injection and Rejection) at PCC	52
5.2.2 Three Phase Dead Short Circuit Fault at PCC	53
5.3 BESS with Adaptive Hybrid Controller (FLC-ANFIS) Emulating VI	54
5.3.1 Sudden Load Variations (i.e. Load Injection And Rejection) at PCC	54
5.3.2 Three Phase Dead Short Circuit Fault at PCC	58
5.4 Comparative Analysis	62
5.5 Discussions	64
Chapter-6: Conclusion and Future Works	65
6.1 Conclusion	65
6.2 Scope of the Future Work	65
References	66

LIST OF FIGURES

Fig. No.	Caption	Page No.
2.1.	Projected RE contribution to the world total energy consumption by 2030.	6
2.2.	The applications of conventional SM and VI-based inverters.	9
2.3.	A basic control scheme for grid forming inverters.	10
2.4.	Grid forming inverter, with additional current and voltage control loops.	10
2.5.	A basic control scheme for grid feeding inverters.	11
2.6.	Grid supporting inverter operating as a voltage source.	12
2.7.	The implementations of VI emulation technique	13
2.8.	The effect of VI that reduces sudden frequency drop	14
2.9.	The VI-based inverter enables the imitation of conventional SG-based power system.	14
2.10.	The typical connection of a generic VI-based inverter	15
2.11.	The block diagram of a generic VSM control strategy to emulate VI	15
2.12.	The general control strategy of a VSG.	16
2.13.	The active power loop for a VSG	16
2.14.	The reactive power loop for a VSG.	17
2.15.	Power system with emulated virtual inertia with synchronverter	17
2.16.	Control architecture of original synchronverter	18
3.1.	Control Scheme of Grid Forming Inverters (Without current or voltage control loop)	23
3.2.	Control Scheme of Grid Forming Inverters (With current or voltage control loop)	24
3.3.	MATLAB/SIMULINK implementation of the grid connected PV system	24
3.4.	Grid connected PV array (a) multi-stage and (b) single-stage	25

3.5.	Simulation results for case study-1 (a) DC link voltage at the inverter input (b) Power produced by solar PV array (c) Power absorbed/delivered by the grid (d) Power delivered by the inverter (e) Load power demand and (f) Frequency of the grid at PCC	28
3.6.	Varying irradiance (W/m ²) at the input of solar PV module	29
3.7.	Simulation results for case study-2 (a) DC link voltage at the inverter input (b) Power produced by solar PV array (c) Power absorbed/delivered by the grid (d) Power delivered by the inverter (e) Zoomed version of Fig. 3.7.(c)-dq0 Controlled (f) Zoomed version of 11(d)-dq0 Controlled (g) Load power demand and (h) Frequency of the grid at PCC	30
3.8.	Simulation results for case study-3 (a) DC link voltage at the inverter input (b) Power produced by solar PV array (c) Power absorbed/delivered by the grid (d) Power delivered by the inverter (e) Load power demand and (f) Frequency of the grid at PCC	31
3.9.	Simulation results for case study-4 (a) DC link voltage at the inverter input (b) Power produced by solar PV array (c) Power absorbed/delivered by the grid (d) Power delivered by the inverter (e) Zoomed version of Fig. 3.9.(c)-dq0 Controlled (f) Zoomed version of Fig. 13(d)-dq0 Controlled (g) Load power demand (h) Frequency of the grid at PCC (i) Zoomed version of Fig. 3.9.(h)-dq0 Controlled (j) Zoomed version of Fig. 3.9.(h)-Conventional Controlled	33
3.10.	Simulation results for case study-3 (a) DC link voltage at the inverter input (b) Power produced by solar PV array (c) Power absorbed/delivered by the grid (d) Power delivered by the inverter (e) Load power demand (f) Frequency of the grid at PCC and (g) Zoomed version of Fig. 3.10.(f)	35
3.11.	Simulation results for case study-3 (a) DC link voltage at the inverter input (b) Power produced by solar PV array (c) Power absorbed/delivered by the grid (d) Power delivered by the inverter (e) Load power demand and (f) Frequency of the grid at PCC	36

4.1.	System configuration of the proposed system connected to a low inertia grid.	38
4.2.	Membership functions plot of input variable (Frequency Error)	39
4.3.	Membership functions plot of input variable (ROCOF)	39
4.4.	Membership function plot of output variable (Adaptive Current Reference)	40
4.5.	Three-dimensional surface plot of fuzzy inference system rules.	40
4.6.	Rules viewer of fuzzy logic inference system.	41
4.7.	Basic structure of ANFIS model for two inputs	42
4.8.	Rules viewer and surface view plot of the ANFIS model	44
4.9.	Typical diagram of a battery equivalent circuit model.	45
4.10.	Nominal discharge characteristics plot of the Battery.	46
4.11.	Grid connected bi-directional converter and inverter.	47
4.12.	Matlab/Simulink implementation setup of the proposed system	48
4.13.	Adaptive hybrid BESS controller implementation in Matlab/Simulink	49

4.14.	Power flow control of the BESS using DC-DC bidirectional converter.	50
5.1.	Case study analysis flow diagram	51
5.2.	Sudden load variation (a) Grid frequency at PCC and (b) Rate of change of frequency (ROCOF)	52
5.3.	Three phase short circuit fault (a) Grid frequency at PCC and (b) Rate of change of frequency (ROCOF)	53
5.4.	Sudden load variation (a) DC link voltage (b) Adaptive current reference of BESS controller (c) BESS voltage and (d) State of charge (SOC) of BESS	55
5.5.	Sudden load variation (a) Current injected by BESS (b) Active power supplied or absorbed by BESS (c) Reactive power supplied or absorbed by BESS (d) Grid frequency at PCC (e) Rate of change of frequency (ROCOF) and (f) Adaptive defuzzified value of FLC	57
5.6.	Three phase short circuit fault at PCC (a) DC link voltage (b) Adaptive current reference of BESS controller (c) BESS voltage and (d) State of charge (SOC) of BESS	59
5.7.	Three phase short circuit fault at PCC (a) Voltage at PCC (b) Current injected by BESS (c) Active power supplied or absorbed by BESS (d) Reactive power supplied or absorbed by BESS (e) Grid frequency at PCC (f) Rate of change of frequency (ROCOF) and (g) Adaptive defuzzified value of FLC	62

LIST OF TABLES

Table No.	Caption	Page No.
3.1	Specifications of parameters of the dq0 based grid forming inverter	26
4.1	Fuzzy rules used for proposed controller	41
4.2	Specifications of Battery and Inverter	47
5.1	Comparative analysis between FLC-PI and FLC-ANFIS based BESS controller performance	63
5.2	Comparison of the performance of FLC-ANFIS based BESS controller with related works	64

LIST OF ABBREVIATIONS OF TECHNICAL SYMBOLS AND TERMS

Abbreviation/symbol	Meaning
AGC	Automatic Generation Control
ANFIS	Adaptive Neuro Fuzzy Inference System
ANN	Artificial Neural Network
BESS	Battery Energy Storage System
BMS	Battery Management System
BSA	Backtracking Search Algorithm
DFIG's	Doubly Fed Induction Generator's
EIC	Emulated Inertia Control
ESS	Energy Storage System
HVDC	High Voltage Direct Current
IAMs	Integrated Assessment Models
IEA	International Energy Agency
MMC	Modular Multilevel Converter
MPC	Model Predictive Control
PCC	Point of Common Coupling
PCRET	Pakistan Council of Renewable Energy Technologies
PSO	Particle Swarm Optimization
RePL	Reactive Power Loop
RESs	Renewable Energy Sources
ROCOF	Rate of Change of Frequency
RPL	Real Power Loop
SDGs	Sustainable Development Goals
SMs	Synchronous Machines
SOC	State of Charge
SPWM	Sinusoidal Pulse Width Modulation
STATCOM	Static Synchronous Compensator
THD	Total Harmonic Distortion
TOU	Time of Use
VSG	Virtual Synchronous Generator

ACKNOWLEDGEMENT

At first, I would like to remember ALLAH, the Almighty with due respect. I want to thank the almighty ALLAH for giving me the opportunity to conduct my thesis. It has become possible to reach the destination because of His grace and mercy. It is a great pleasure for me to express unfettered gratification, sincere appreciation and profound respect to my supervisor Dr. Abdul Hasib Chowdhury, Professor, Department of Electrical and Electronic Engineering, Bangladesh University of Engineering and Technology, Bangladesh, for his constructive suggestion, guidance, constant inspiration, and kind co-operation throughout the entire progress of this thesis work. It would have been impossible for me to accomplish my work without his remarkable advices.

I would also like to thank all of my course-work faculties of Department of Electrical and Electronic Engineering, Bangladesh University of Engineering and Technology, Bangladesh. I extend my gratitude and appreciation to my respected and beloved parents as well as my wife for their cooperation, patience and faith on me to complete my thesis successfully. Finally, I wish to thank all the concerned teachers and staffs and my respected group members of the department for their direct and indirect assistance at different events of the work.

ABSTRACT

Due to the rapid increasing demand of grid connected solar photovoltaic, the overall system inertia decreases and hence causes system instability. Virtual inertia emulation is one of the solution to this low inertia problem that can be done through inverter control and energy storage devices. This thesis presents a simple improved adaptive Fuzzy-ANFIS hybrid algorithm-based BESS controller that can emulate virtual inertia to improve frequency stability of a low inertia grid. The proposed controller has been tested on a low inertia grid for different case studies and a comparative analysis has been done in the last chapter of this thesis. The presented controller eliminates the limitations of conventionally used PI controller and hence an improvement of frequency nadir by 0.43% for sudden load variation and 0.61% for transient short circuit fault have been observed. Moreover, improvement in ROCOF and settling time have been noticed for the proposed controller also.

Chapter-1

Introduction

1.1 Motivation

Inertia is the term used to describe the energy that is stored in big rotating generators and some industrial motors, giving them the tendency to continue rotating. The stored energy also counterbalances supply and demand imbalances on electricity networks over very short time periods. Traditional power systems are made up of sizable power plants with synchronous machines (SMs), which provide the system a lot of inertia. However, in recent years there has been a noticeable growth in the number of renewable energy sources (RESs). The dynamics of the power system are significantly altered when increasing penetrations of inverter-based resources—e.g., wind and solar photovoltaics (PV)—that do not naturally provide inertia. As more renewable resources are installed replacing the conventional fossil fuel-based generators that have high inertia, the overall system inertia is continuously declining. This emerging grid is frequently referred to as a low-inertia power system.

The grid frequency, f is directly coupled to the rotational speed of a synchronous generator and thus to the active power balance. Rotational inertia, i.e. the inertia constant H , minimizes change in Δf in case of frequency deviations. The reduced inertia in the power system leads to an increase in the rate of change of frequency (ROCOF) and frequency deviations in a very short time, under power imbalances and causes stability issues like frequency instability, voltage instability, power oscillations etc. By preventing frequency variations, inertia in power systems contributes significantly to preserve the stability and reliability of the system. Hence, there should be some technology that can emulate inertia from the zero inertia renewable energy sources. The idea of virtual inertia has evolved in order to address the problems associated with low inertia in power electronic-based power systems. Virtual inertia is the addition of extra electrical power from a source that does not naturally release energy when the frequency of its terminal frequency varies but that mimics the release of kinetic energy from a rotating mass. This concept is realized by using a control function interfaced with power electronics to

simulate synchronous machines inertial dynamics and provide the inertia virtually. Virtual inertia can be emulated in a low inertia grid by using inverter control and energy storage elements like DC link capacitor, supercapacitor, ultracapacitor, BESS etc.

Inverter control algorithm like droop control, virtual synchronous generator (VSG) technology, synchronverter etc. have been widely used for both RESs integrated low inertia grid and microgrid system to emulate virtual inertia and enhance system stability. But, the limitation of the control system of the inverter is its complexity since, the inverter should mimic the behaviour of a synchronous machine. Battery Energy Storage System are mainly used in microgrid system for frequency stability enhancement that uses fuzzy logic and PI controller for designing their control system taking active and reactive power deviation at point of common coupling (PCC), frequency deviation, BESS state of charge (SOC) etc. as inputs to provide inertial support. But the PI controller has the disadvantages of higher settling time, slower response, more oscillations and parameters are not adaptive in nature.

1.2 Objectives

The objectives of this thesis are the following:

- i. To develop adaptive BESS controllers for enhancing frequency stability of a low inertia grid.
- ii. To evaluate and compare the performance of the proposed controllers.

1.3 Methodology

The proposed controller will be capable of injecting or absorbing active power based on the frequency deviation and rate of change of frequency (ROCOF) to keep the system stable under different abnormalities. The amount of active power injection or absorption will be also adaptable depending on the value of ROCOF to ensure better control on the system frequency. The first part of this work will be to design the inverter controller. DQ0 based grid following inverter topology will be implemented. The inverter will provide active power support only since the primary

objective of the work is to enhance frequency stability. The second part of the work will be to design an adaptive BESS controller for grid level application that can emulate virtual inertia for providing inertial support to the low inertia grid. Fuzzy logic controller (FLC) and PI controller will be implemented based on the frequency deviation and ROCOF as inputs and BESS current reference as the output. The parameters of the PI controller will be extracted from auto tuning option of MATLAB/Simulink that utilizes Particle Swarm Optimization (PSO) technique to get the best response. The adaptive nature of the FLC ensures the adaptive control of the active power flow from the BESS. The third part of this work will be to develop an improved adaptive BESS controller that overcomes the limitations imposed by the PI controller under transient events. The proposed FLC-PI controller will be modified by replacing the PI controller with adaptive neuro fuzzy inference system (ANFIS) and develop an FLC-ANFIS controller. The final part of this work will be to test, evaluate and compare the performance of the proposed BESS controllers (i.e. FLC-PI and FLC-ANFIS) from the perspective of frequency nadir and ROCOF under different abnormal grid scenarios at PCC.

1.4 Thesis Outline

Chapter 2 will focus on the literature review. The growing utilization of RESs and its integration with the existing grid, low inertia problems and its effects on system stability, inverter control architectures, BESS applications for inertial improvements etc. have been reviewed in this chapter.

Chapter 3 will discuss the control architecture of DQ0 transformation along with its applications for inverter control in grid connected RESs. A simple case study has been presented in this chapter to show the potentiality of the controller to keep the system stable.

Chapter 4 will highlight the actual design of the proposed improved BESS controller that can simulate virtual inertia for enhancement of frequency stability of a low inertia grid. The components specifications along with the simulation setup have been discussed in this chapter.

Chapter 5 will present the simulation results of the studied system utilizing the proposed controller under different case studies. The obtained results will be discussed and a comparison will be presented in this chapter.

Chapter 6 is the conclusion section, where we shall formally terminate the thesis with concluding remarks. Furthermore, the direction of the future research will be highlighted at the end.

Chapter-2

Literature Review

2.1 Renewable Energy

Since human civilization almost depends on the energy extract from fossil fuel (80% according to IEA), massive scale use of fossil resources increases the risk of environmental degradation. Hence, the world is shifting towards the utilization of maximum renewable energy sources for minimizing the dependency on fossil fuel-based generation. The term “renewable energy” has been used as “inexhaustible fossil fuel” since early 1900s but later on animal power sources and wood have been termed as “renewable” while solar, wind, tidal and hydro have been termed as “inexhaustible”. According to The International Energy Agency (IEA), the renewable energy is defined as “energy derived from natural processes that are replenished at a faster rate than they are consumed” [1]. Due to the production of greenhouse gas (GHG) like CO_x, NO_x and SO_x etc. from burning of fossil fuel, the use of RESs has drawn the attention of the whole world especially wind and solar photovoltaic cells [2]. Renewable energy generation can be both centralized and decentralized. As a result of less energy density of most of the renewable energy sources, the generation of renewable energy will be more decentralized which will lead towards mentionable variations in the regional economy [3]. Due to the rapid increase of the demand for energy and concern for reducing environmental pollutants like CO₂ emissions from fossil fuels like oil, coal, gas etc.; renewable energy sources have drawn the attention of the policy makers, researchers and additionally the consumers of the world [4]. China has targeted to limit its carbon emissions per unit of gross domestic product by 60-65% by the year 2030 [5]. The United Nation (UN) has set 17 Sustainable Development Goals (SDGs) for ensuring the sustainable development of countries by 2030 [5], [6]. The definition of sustainable development is stated as, “maintaining the amount of the sources used by the society for today’s needs at a level that will not deprive future generations of their needs”. Hence, for achieving the goals set by UN, the use of renewable energy should be increased compared to non-renewable energy sources [6], [7]. One of the studies by the World Outlook and integrated assessment models (IAMs) predicted that the contribution of renewable energy to the world’s

primary energy will be 20-30% by 2040. The study also suggested that it is possible theoretically to switch toward a completely renewable based energy system by 2050 [8]. It is expected that the world will meet total 36% of its energy demand from RESs by 2030 as shown in Fig. 2.1 [9].

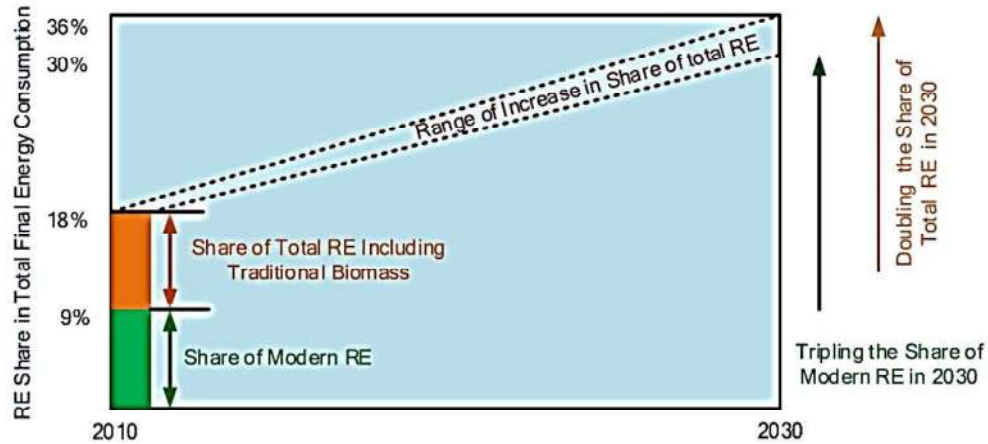


Fig. 2.1. Projected RE contribution to the world total energy consumption by 2030.

In one of the studies, it is stated that by 2035, India will be the second largest contributor to global energy demand as proposed by IEA. The country has aimed to extract 175 GW of energy from renewable sources especially from solar photovoltaic and wind energy by 2022 [10]. Another study in Pakistan showed that, from 2015 to 2020, the investment of the government increased many a times in the renewable energy sector (especially hydro based generation) to balance between supply and demand. Also, Pakistan Council of Renewable Energy Technologies (PCRET) started to conduct training sessions for the people of its country for encouraging them to use RE based devices like solar cooker [4]. European Union (EU) as the most vulnerable countries/unions due to its high dependency for energy imports. The large differences between the production and consumption of fossil fuels push EU to import 54% of total energy consumed by the countries. Hence, EU has a target to produce RE of 27% of the total energy by 2030 [11]. In Latin America, more than 50% of the total generation comes from hydropower where in United States and the Asia-Pacific region, the contribution of renewable energy is almost 18%. In Canada, about 64% of the total generation by the country comes from renewable energy sources and the country expects to raise the percentage to 70% by 2025 [12]. The Government of Malaysia in 2018 set its target to achieve renewable energy penetration of 20% by 2025 and to reduce the emissions of GHG intensity of Gross Domestic Product (GDP) by 45% by 2030. The country has targeted to reduce dependency on fossil fuels in

the eleventh Malaysia Plan (2016-2020) by increasing RE levels [13]. 100% renewable energy concept has allured different countries like Sweden, Denmark, Barbados, Cambodia, Colombia etc. including Bangladesh to achieve almost zero net emissions of GHG by 2045 or 2050. The authors concluded that by exchanging potentials renewable energy resources among certain regions of a country, a region with limited renewable resources can adopt 100% RE transition [7]. Moreover, another study in Africa showed that, three countries of Africa namely South Africa, Egypt and Nigeria have started to implement renewable energy projects to reduce the dependency on oil. Egypt has set its target of generating 700 MW from solar PV by 2027 where Nigeria has targeted to generate 500 MW by 2025. South Africa has planned to reach a target of generating 8.4 GW from solar PV by 2030 [14]. The investment in the renewable energy sector has been boosted by 17% due to the technological developments and reduction in the cost [7], [15] for installations (according to the World Energy Outlook 2019).

2.2 Low Inertia Grid and System Stability

Traditional power systems are made up of sizable power plants with synchronous machines (SMs), which provide the system a lot of inertia. However, the number of RESs has increased noticeably in recent years. Increased penetration of inverter-based resources—such as wind and solar photovoltaics (PV), which do not naturally supply inertia—alters the dynamics of the power system dramatically [16]. The inertia of the entire system is continuously decreasing as additional renewable resources are installed to replace existing, high-inertia generators powered by traditional fossil fuels, nuclear power, and hydropower [17]. Among all the RESs, with an estimated 5600 ZJ (Zettajoule) of yearly worldwide insolation, solar PV based generation has grown exponentially since the financial expenses have dropped significantly as a result of advances in the materials used to create PV cells [18]. The reduced inertia in the power system due to the zero inertia and intermittent nature of PV, leads to an increase in the power imbalances, power oscillations, frequency nadir and ROCOF and hence effects the system stability, security and protection [19]-[22].

Due to the unidirectional power flow structure of distribution grid, operational problem arises mainly for the PV system without any reactive power support. Large integration of RE sources accelerates stability problems like voltage stability, rotor angle stability (i.e.

transient and small signal stability) and frequency stability [22], [23]. A study in IEEE-39 bus test system reveals that beyond a certain limit of injecting PV based generation causes instability in slack bus power along with momentary voltage, frequency fluctuations in response to any transient event [24]. Wind based generation contributes very less to the system inertia where PV has no inertia contribution due to the de-coupling through PE converters and hence the overall system inertia reduces [21], [22] due to large scale integration of RESs. Lowering system overall inertia accelerates frequency instability as well as causes the value of ROCOF to increase. Also, the power quality degrades due to the injection of harmonics by the PE converter at the PCC resulting in higher total harmonic distortion (THD) value, flickers and transients etc. [25]. The authors in [26] have investigated the impact of centralized and distributed PV generation on a realistic distribution system on grid stability and found that centralized PV integration affects more on system stability than the distributed PV integration. Grid connected PV systems have significant impacts on the system stability and protection system due to the intermittent nature and the case is worst in case of standalone or weak grid system as reported in [21], [22], [27]. The overall instability of a grid-connected inverters is due to the control loops instability and inverter output voltage instability. The non-linear behaviour of different components of the control loops lead to instability issues [28].

2.3 Inverter Control and Virtual Inertia Emulation

The idea of virtual inertia has evolved in order to address the problems associated with low inertia in RESs-based power systems [29]. Many researchers have proposed virtual inertia emulation techniques to enhance grid stability based on the inverter control algorithm that mimic the behaviour of a synchronous machine to provide inertial support to a weak grid. Droop control, virtual synchronous generator (VSG) technology, synchronverter etc. are the recently proposed control algorithm that can simulate synthetic inertia from a zero inertia RESs [30]. However, the aforementioned inertia emulation techniques provide inertia to the system, but the challenge is to provide voltage and frequency support for the system. Moreover, since most of the recently proposed controllers are modelled based on the swing equation, the system may face stability issues that depends on the type of disturbances [31].

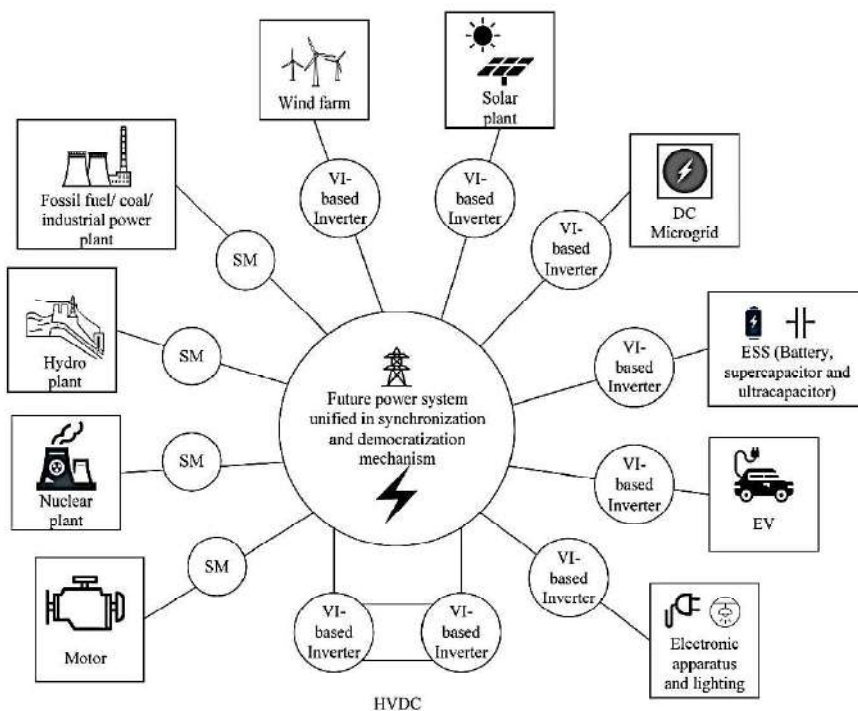


Fig. 2.2. Applications of conventional SM and VI-based inverters.

Fig. 2.2 shows the applications of conventional synchronous machines and virtual inertia-based grid connected inverters. Three typical modes of operation of grid-connected inverters are grid forming, grid feeding, and grid supporting. The selected mode of operation determines the inverter dynamics, and its steady-state characteristics.

2.3.1 Grid Forming Inverters

Grid forming inverters are typically used in small isolated networks, and their main objective is to regulate the network voltage and frequency. To this end, grid forming inverters are controlled as voltage sources, with fixed voltage amplitude $|E|$ and frequency ω . The active power P and reactive power Q are not directly controlled, and are determined by the interaction of the inverter with the network. Typical applications are standby uninterruptible power supply (UPS) systems, and islanded microgrids. Since the frequency ω is set, the inverter usually can operate in parallel to other grid forming inverters when an additional mechanism matches the frequencies. In power flow studies, a grid forming inverter may be viewed as an infinite bus, and is represented as a reference bus, with a constant voltage amplitude $|E|$ and angle $\delta = 0$. Grid forming inverters are also called Voltage Source Inverters (VSI) [62]. A basic control scheme of grid forming

inverters is shown in Fig. 2.3 and its improved version that incorporates current and voltage control loop is shown in Fig. 2.4.

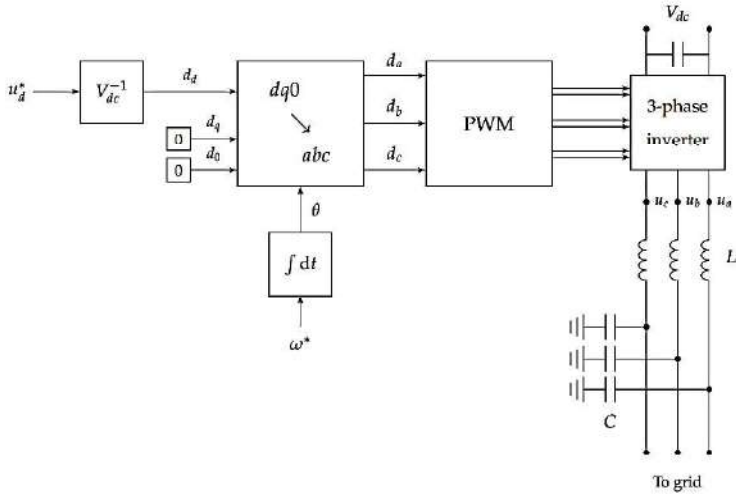


Fig. 2.3. Basic control scheme for grid forming inverters.

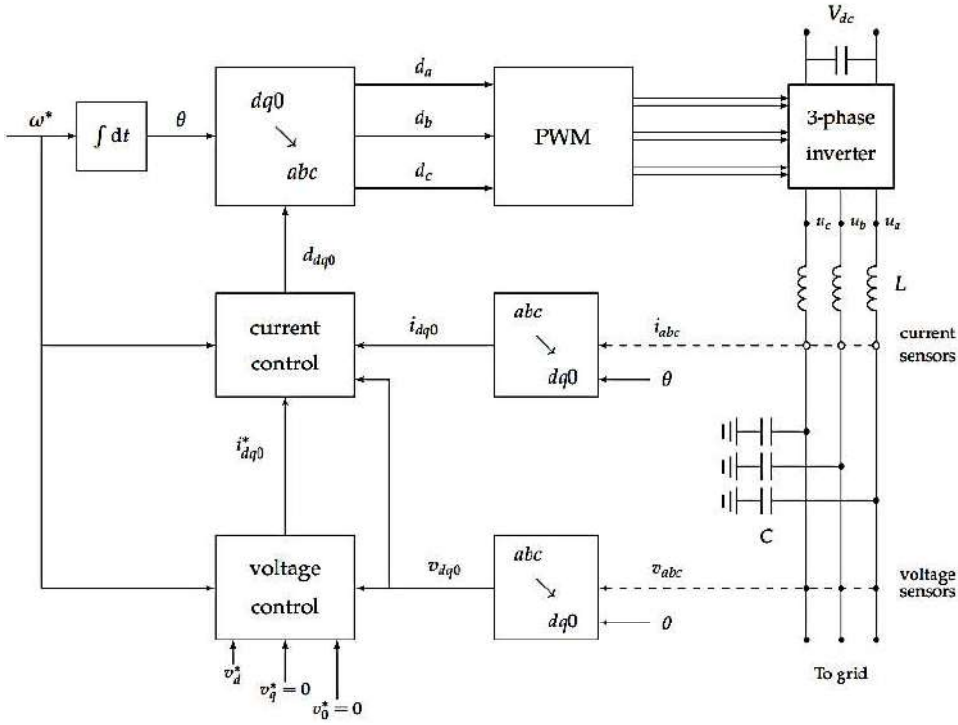


Fig. 2.4. Grid forming inverter, with additional current and voltage control loops.

2.3.2 Grid Feeding Inverters

Grid feeding inverters are operated as power sources, and are mainly designed to deliver power to an energized grid. The active power P and reactive power Q are directly controlled, while the frequency ω and voltage amplitude $|E|$ are not directly controlled, and are determined by the interaction of the inverter with the grid. Typical applications are renewable energy systems and small grid-connected generators, which operate with specific active and reactive powers. As an example, in photovoltaic systems the active power is typically set by the source, and the reactive power is often set to zero. Grid feeding inverters are designed to operate in parallel to other inverters and generators. They cannot operate in isolation, and require additional units to set the voltage magnitude and frequency. In power flow studies, a grid feeding inverter is represented as a P-Q bus, with constant active power P and constant reactive power Q . Grid feeding inverter are also called Grid Following Inverters, or inverters with P-Q control [62]. The basic control scheme of grid feeding inverters is shown in Fig. 2.5.

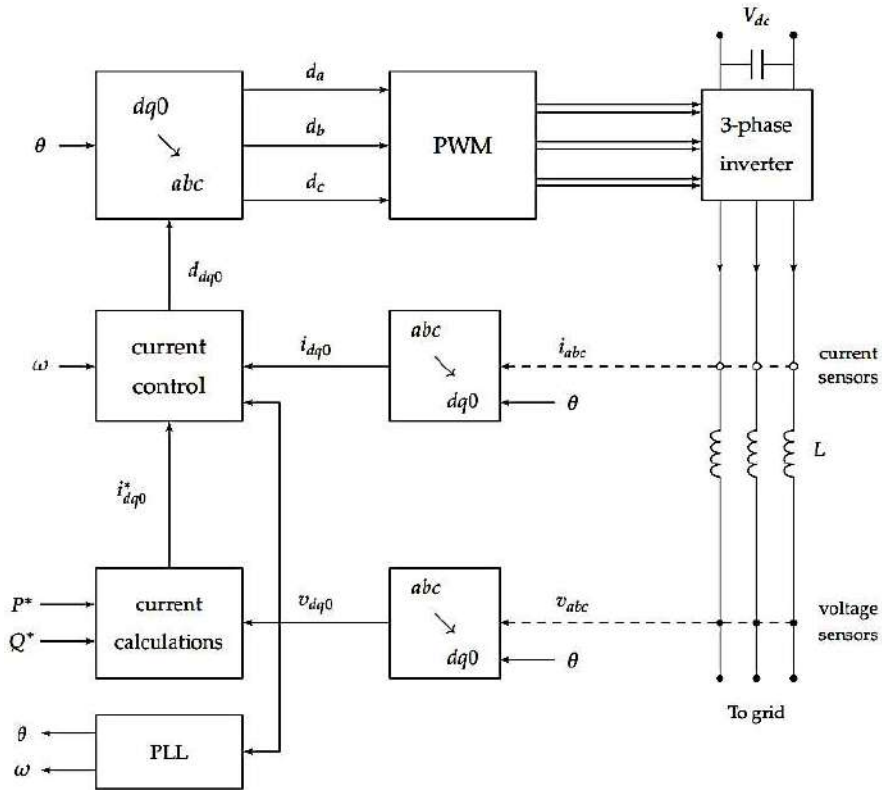


Fig. 2.5. Basic control scheme for grid feeding inverters.

2.3.3 Grid supporting inverters

Grid supporting inverters operate somewhat similarly to synchronous generators: they deliver power to the grid, while contributing to the stability and reliability of the system. The frequency and voltage magnitude are controlled by a droop mechanism, such that there is a linear relationship between ω and P, and between $|E|$ and Q. This type of control promotes fair sharing of the active and reactive powers among generators, while regulating the frequency and voltage. Grid supporting inverters may be connected in parallel to other generators, and can operate in isolation. In power flow studies, such an inverter cannot be represented as a standard bus. However, if the frequency ω is known, and the voltage droop mechanism can be ignored, then the inverter is represented as a P-V bus with constant active power P and voltage amplitude $|E|$, similarly to a synchronous machine [62]. The basic control scheme of grid supporting inverters is shown in Fig. 2.6.

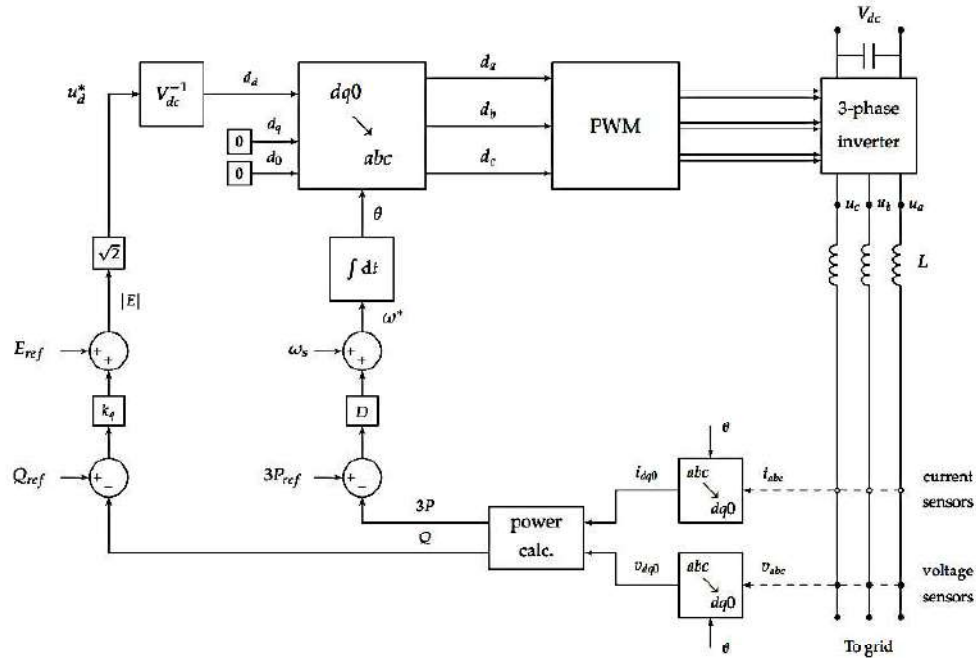


Fig. 2.6. Grid supporting inverter operating as a voltage source.

2.3.4 Virtual Inertia Emulation Techniques

Now-a-days, the inertial support to a low inertia microgrid system is done by modifying the inverter control algorithm based on swing equation to mimic the behaviour of a synchronous machine. The VSG has been reported to be an emerging technology that is widely used for microgrid (MG) systems also to emulate virtual inertia (VI) and enhance

system stability. The authors in [32] proposed a delay-based inverter control strategy that can emulate virtual inertia operating in islanded mode. For a VSG driven inverter-based MG system, a data-based optimization technique has been used in reference [33] that allows the emulated inertia constant to be changed based on the frequency of the MG.

VI-based inverters and their control strategy can be implemented in various applications such as grid-connected wind power and solar power plant, high voltage direct current (HVDC) transmission, energy storage system (ESS), microgrid, electric vehicle (EV) chargers, static synchronous compensator (STATCOM), virtual inertia machine (VIM), modular multilevel converter (MMC)-based direct current (DC) system, electronic appliances, and flexible loads to support frequency stability. Fig. 2.7 presents the application and implementation of VI in the modern power system.

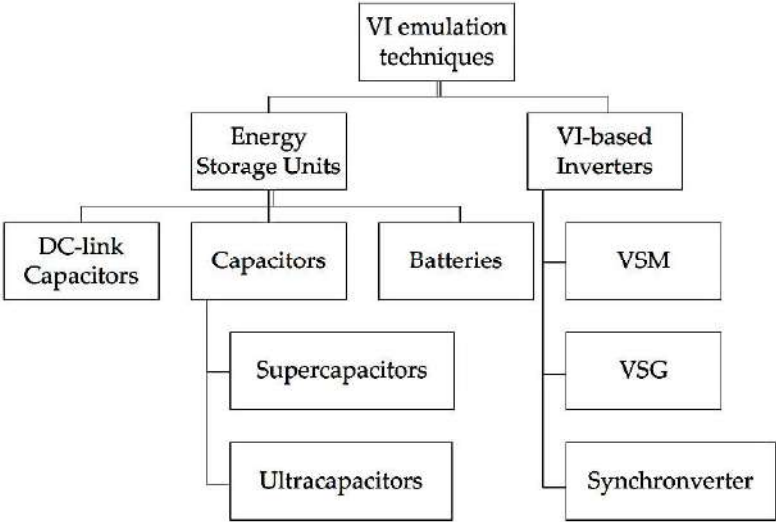


Fig. 2.7. Implementations of VI emulation technique

The power system with VI has the following advantages:

1. Reduction in frequency nadir and frequency deviation from nominal frequency (f_n)
2. Less overshoot and faster transient or respond time.
3. Less ROCOF and less steep gradient
4. Faster recovery time to the nominal frequency

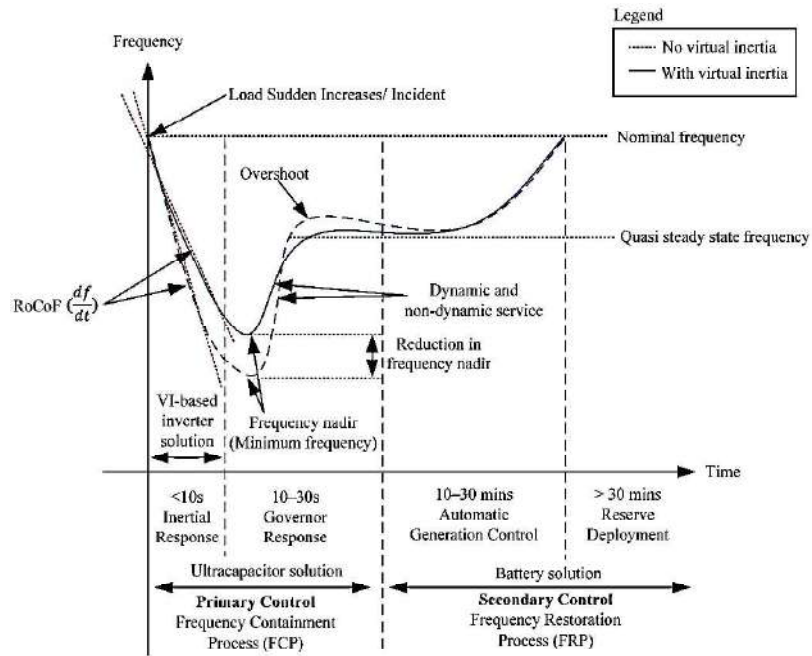


Fig. 2.8. Effect of VI that reduces sudden frequency drop [34].

Fig. 2.8 shows the impact of low inertia on grid frequency under any abnormal scenario. The ROCOF and frequency nadir increases with reduced inertia as seen from the diagram. VI helps to reduce the value of ROCOF and frequency nadir. Fig. 2.9 shows an analogy between conventional high inertia synchronous machine and zero inertia renewable energy sources with inverter that mimics synchronous machine enabling virtual inertia. The typical control system of a virtual inertia emulated inverter has two loops name as active power loop and reactive power loop that helps to generate the required control signal for pulse width modulation (PWM) inverter as shown in Fig. 2.10.

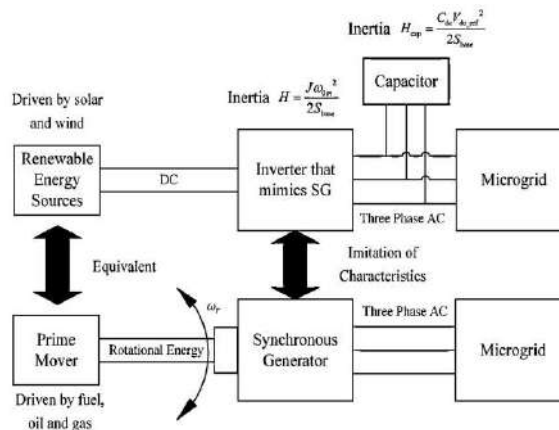


Fig. 2.9. VI-based inverter enables the imitation of conventional SG-based power system.

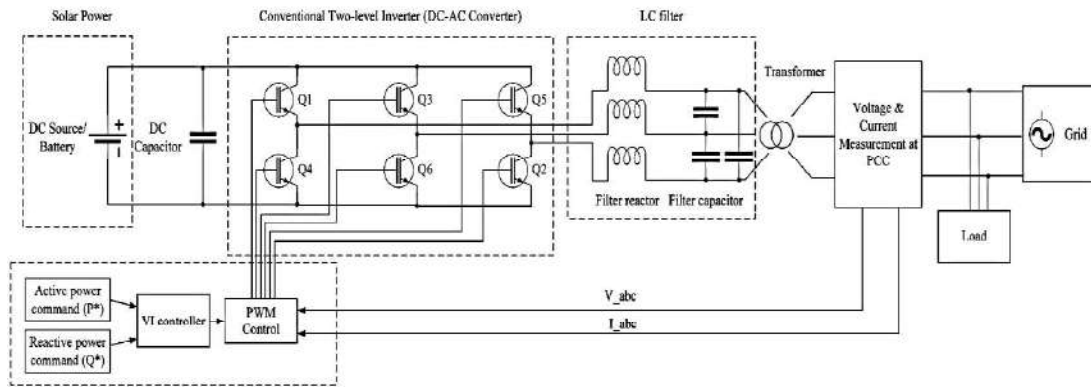


Fig. 2.10. Typical connection of a generic VI-based inverter

Both VSM and VISMA are abbreviations for the virtual synchronous machine. However, VSM is more commonly used. Both are based on the emulation of SM but with some slightly different implementation topology. Various researchers refer to different abbreviations, but essentially VSM and VISMA are interchangeable terms. Although the terms are different, all of them shares similar VI emulation techniques. The objective of the VSM is to provide grid forming employing frequency droop and virtual inertia. A phase locked loop (PLL) is typically used for frequency estimation to calculate the RoCoF in driving the VI loop as shown in Fig. 2.11. The use of PLL is eliminated during regular operation. It is because VSM can synchronize with the grid based on the power balance after initialization by PLL.

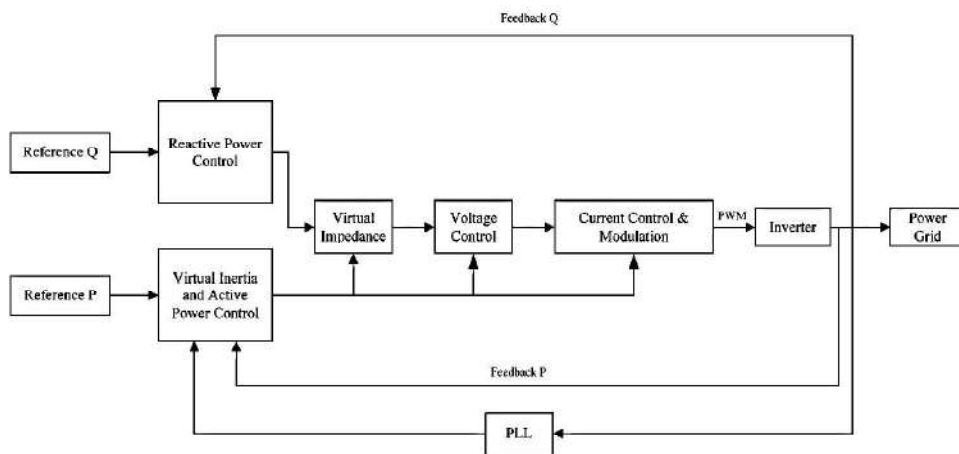


Fig. 2.11. Block diagram of a generic VSM control strategy to emulate VI [35]

VSG is essentially based on conventional inverter hardware with a controller that emulates the inertial response of an SG in response to any frequency changes. VSG control strategy allows the operation of grid-connected inverters to produce VI. The adoption of VSG has attracted significant attention because of its equivalent operating mechanism as an SG to provide a practical scheme for grid-connected RES. The emulation of releasing or absorbing kinetic energy imitates the characteristic of an SG. VSG is different from SG in terms of the ability to modify VI by the microprocessor during frequency variation. Hence, self-tuning algorithms are crucial to vary the VI to minimize frequency variation. Compared to a conventional droop controller that provides frequency regulation only, VSG provides dynamic frequency control based on the derivative of the frequency measurement. This control is similar to the inertial power release or absorption by an SG during a power imbalance. VSG requires pre-synchronization before connecting to the power grid. It is executed by either a conventional PLL or phase angle regulator. The generalized control strategy of a VSG is shown in Fig. 2.12.

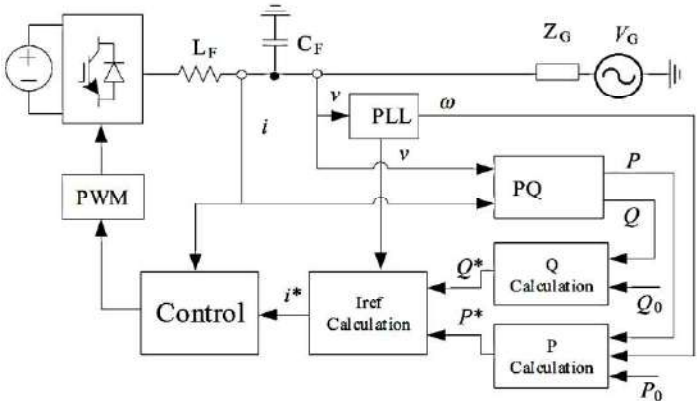


Fig. 2.12. General control strategy of a VSG.

The active and reactive power loop in VSG produces total power (P_T) and output voltage (V_0) based on the frequency deviation and reactive power deviation as seen from the Fig. 2.13 and Fig. 2.14 respectively.

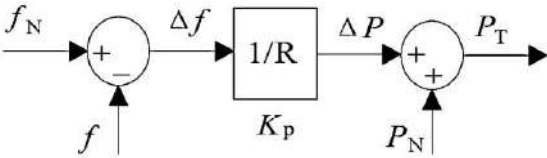


Fig. 2.13. Active power loop for a VSG.

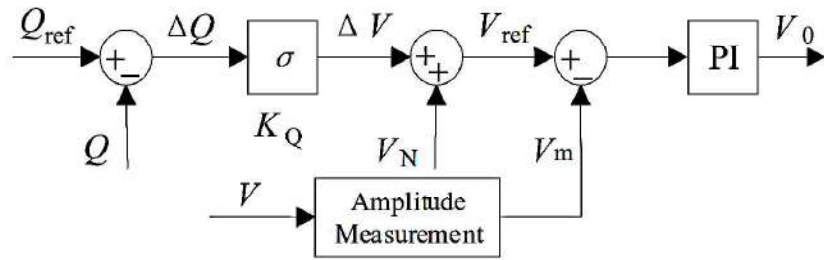


Fig. 2.14. Reactive power loop for a VSG.

The controller produces reference signal for the sinusoidal pulse width modulation (SPWM) to generate six gate pulses for the PWM inverter. Moreover, recent synchronverter technology helps to emulate virtual inertia that works on the modified swing equation of synchronous machine. The applications of synchronverter in modern low inertia power system with renewable and distributed generation is shown in Fig. 2.15.

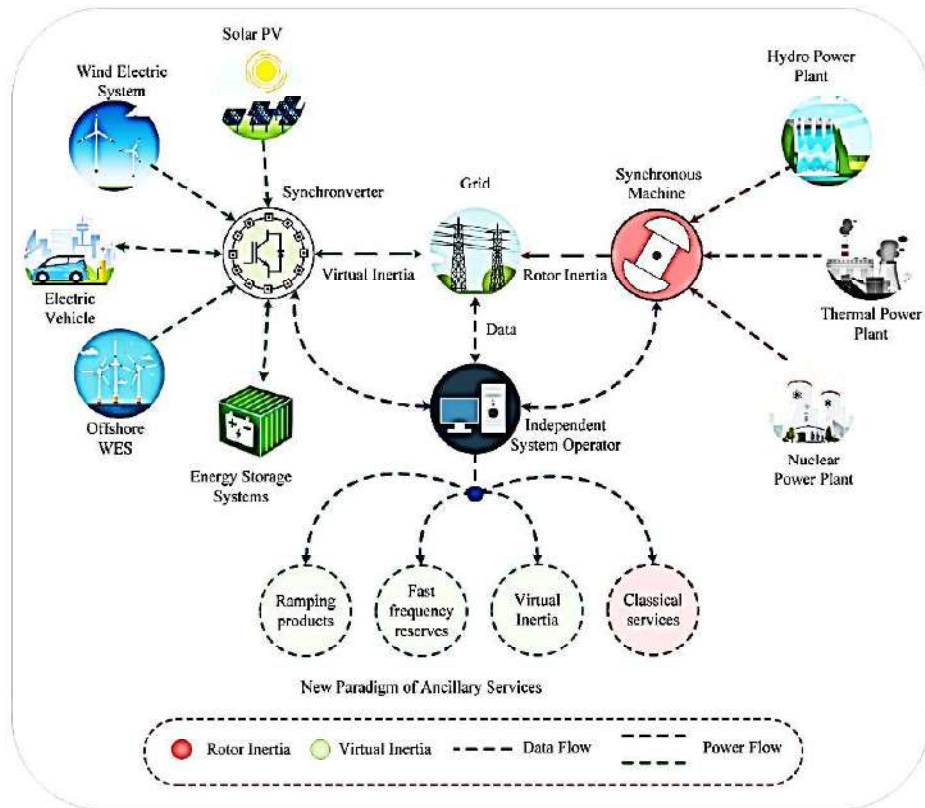


Fig. 2.15. Power system with emulated virtual inertia with synchronverter

To mimic the overall behavior of SM, the empirical model has been augmented with the real power loop (RPL) and reactive power loop (RePL) as shown in Fig. 2.16. The power regulation control has a cascaded structure with the inner and outer loops. As a rule of

thumb, the interior loops are tuned to have higher bandwidth than the outer loops, to achieve the steady-state operating stability. Moreover, the original synchronverter model has been derived by assuming a high inductive output impedance so that the relationship between $P - f$ and $Q - V$ is valid.

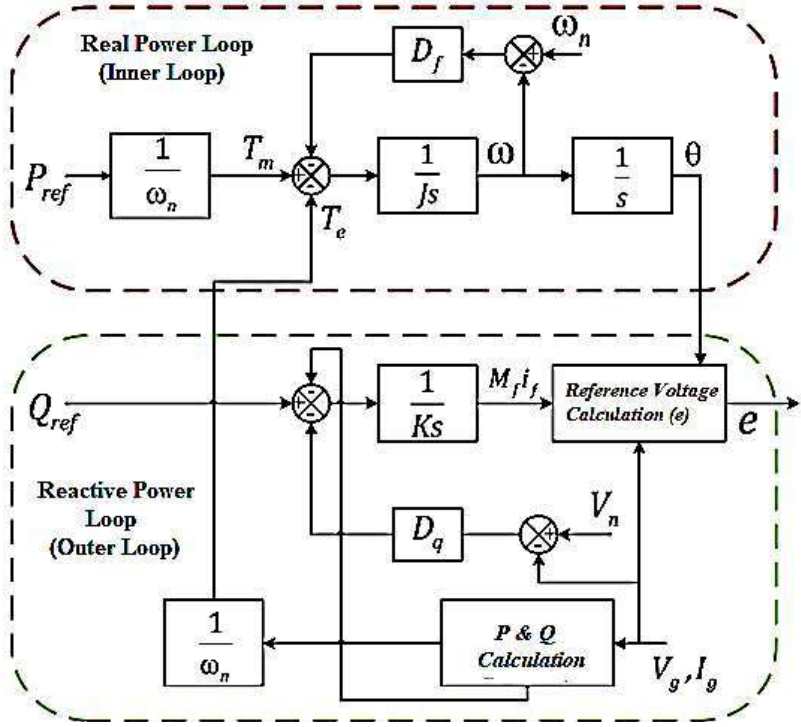


Fig. 2.16. Control architecture of original synchronverter [35]

2.4 BESS Applications for Inertial Improvement

Short term energy storage devices are widely in use to emulate virtual inertia for addressing the low inertia problem. Energy storage elements like DC link capacitor, supercapacitor, ultracapacitor and BESS [36]-[39] have been reported to be used so far by the researchers to simulate virtual inertia and enhance stability of a RESs dominated power system, especially for microgrid applications. DC link capacitor has stability concern during transient events and supercapacitors, ultracapacitors etc. could be employed for the initial frequency response, while not having the capacity to sustain their power output for an extended period of time [40]. Due to having appropriate dynamic properties for frequency support, BESS has been found to be the most prominent technology for the application of stability enhancement of a low inertia grid [41].

For many years, BESS technologies have been employed to lessen the effects of the intermittent nature of renewable energy sources especially for solar PV system. In particular, the widely used microgrid concept are highly prone to system instability during islanded mode and hence BESS is used at PCC for peak shaving or power balancing. Furthermore, BESS has been reported to be used in DC Nano Grid application by the authors in [42] that utilizes DC Bus Signalling (DBS) management technique as a distributed and decentralized control solution. The need for preserving inertia, whether through synchronous or synthetic means, is acknowledged by both researchers and the industry, primarily in order to keep the ROCOF relay settings unchanged [40]. The main challenges are to design a fast acting, adaptive, simple BESS controller that can limit the value of ROCOF and frequency nadir by providing inertial support to ensure grid stability and proper functioning of the protective devices. To effectively employ BESS for an isolated microgrid to control voltage and frequency of the system, many researchers have developed a variety of models and methods for battery management system (BMS). The control architecture of the BMS is frequently designed using fuzzy logic controllers due to its adaptive nature and lack of a requirement for accurate inputs [43]-[52].

Most of the literatures that have been found after study are based on the application of BESS for microgrid applications to improve voltage and frequency stability under both grid connected and standalone mode. Fuzzy logic controller (FLC) based controllers have been demonstrated as a potential solution by many researchers to meet the challenges imposed by a RESs dominated microgrid system. An FLC based on backtracking search algorithm (BSA) has been presented in [44] for controlling the charging and discharging mode of a battery for microgrid applications that depends on the rate of change state of charge (SOC) and power balance. Paper [45] proposes a FLC based method for coordinated BESS control and modified AC coupling topology. The performance has been reported to be better than that of a typical PI-based controller in terms of overshoot, settling time, total harmonic distortion (THD) and other metrics. For the islanded Mae Sariang microgrid, a fuzzy logic controller based on active power and reactive power fluctuations has been suggested in [46] to govern the active and reactive power supplied by BESS. The solution performed excellently when compared to an effective battery controller in order to increase voltage and frequency stability for the islanded microgrid in response to the uncertainties from RESs. The authors of [47] proposed an FLC for standalone microgrid applications using BESS and electric vehicle (EV) to regulate

microgrid frequency and voltages based on the different feedback signals like frequency, DC bus voltage, SOC of BESS and EV etc. The controller showed better performance than the conventional PI based droop control technique.

To improve the resilience of hybrid microgrid systems, a fuzzy logic-based controller has been developed in [48] employing the BESS SOC, event occurrence probability, and market price as input signals. A fuzzy logic-based controller for BESS that is utilized for primary frequency controlling is presented in paper [49]. The algorithm is tested on a transfer function-based BESS model where SOC and energy limits have been considered. For both the grid-connected and islanded modes of operation, the controller modifies the active power from BESS using SOC and power deviation as input. The authors of [50] suggested an FLC with higher economic benefits for BESS and load management in microgrid applications. As suggested in this study, using the time of use (TOU) electricity pricing idea in conjunction with the fuzzy logic algorithm can reduce annual energy costs by 10.96%. For a wind-BESS hybrid system, the authors of [51] suggested a frequency management technique based on FLC. The primary frequency control for lowering the maximum excursion frequency and ROCOF was enabled by the suggested algorithm by using the frequency deviation, ROCOF, wind speed, and SOC as input signals.

Apart from the microgrid concept, several studies have been done where BESS has been used for providing inertial support to a low inertia grid under dynamic condition. According to article [52], doubly fed induction generator's (DFIG's) rotating mass simulating virtual inertia provides the primary frequency control, and an adaptive neuro fuzzy inference system (ANFIS)-based control algorithm supports the secondary frequency control, which mitigates the inherent low inertia problem of RESs integration. Based on three different case studies, the authors of [53] demonstrated that installing BESS on a grid-level transmission system can quickly respond to inertial difficulties caused by the integration of RESs. A novel supercapacitor-based mimicked inertia control technique has been presented in [54] to provide inertial support to a low inertia grid, which outperforms traditional emulated inertia control (EIC) in terms of frequency nadir and ROCOF. According to an analysis in [55], it has been shown that, BESS performs better than static synchronous compensator (STATCOM) when the generator's operational boundary margin is greater and can be used to increase steady state stability. As suggested in [56], BESS can reduce ultra-low frequency oscillation when used in conjunction with automatic generation control (AGC). By removing the need for

cascaded linear control based on PI controller and utilizing model predictive control (MPC), the authors in [57] propose a predictive control scheme for inverters that emulates virtual inertia by tracking the desired ROCOF for various disturbances. A double artificial neural network (ANN)-based controller for VSG inverter has been proposed in [58] that can regulate the inertia parameter to decrease the stress on power semiconductor devices of VSG to ensure system reliability and stability. An improved transient angle stability has been observed by the proposed VSG controller in [59]. Paper [60] proposes a novel virtual induction machine-based synchronization technique replacing the conventional PLL for grid following inverter with low inertia. A novel synthetic inertia controller along with its tuning process of various parameters has been proposed to limit the value of ROCOF [40].

Chapter-3

DQ0 Algorithm Based Inverter Control

3.1 DQ0 Transformation and Inverter Controller

DQ0 transformation converts a signal in a-b-c reference frame to rotating dq0 reference frame and the reference frame conversion makes the analysis under both transient and steady-state conditions easier [62]. The authors of papers [61]-[63] presented different inverter configurations like grid forming, grid feeding and grid supporting on the basis of dq0 transformation. Since dq0 reference frame exhibits better performance under transient and steady state condition, time varying a-b-c reference frame are not used in most of the RE based control system. The dq0 transformation also called as Park's transformation matrix can be given as (1)

$$T_{\theta} = \frac{2}{3} \begin{bmatrix} \cos(\theta) & \cos\left(\theta - \frac{2\pi}{3}\right) & \cos\left(\theta + \frac{2\pi}{3}\right) \\ -\sin(\theta) & -\sin\left(\theta - \frac{2\pi}{3}\right) & -\sin\left(\theta + \frac{2\pi}{3}\right) \\ \frac{1}{2} & \frac{1}{2} & \frac{1}{2} \end{bmatrix} \quad (1)$$

The inverse Park transformation can be done by the following matrix (2)

$$T_{\theta}^{-1} = \begin{bmatrix} \cos(\theta) & -\sin(\theta) & 1 \\ \cos\left(\theta - \frac{2\pi}{3}\right) & -\sin\left(\theta - \frac{2\pi}{3}\right) & 1 \\ \cos\left(\theta + \frac{2\pi}{3}\right) & -\sin\left(\theta + \frac{2\pi}{3}\right) & 1 \end{bmatrix} \quad (2)$$

Applying dq0 transformation to the inverter current injected to the system, the d-axis and q-axis current can be given by (3) and (4).

$$i_d = k_d \frac{3}{2} I_m \sin(\omega_{st} - \theta) \quad (3)$$

$$i_q = -k_q \frac{3}{2} I_m \cos(\omega_{st} - \theta) \quad (4)$$

The system regulates the output voltages such that $v_d = v_d^*$, $v_q = 0$, $v_0 = 0$. This control is implemented by using two loops: an inner loop that controls the currents,

and an outer loop that controls the voltages [61]. The filter inductor equations in the dq reference frame including cross coupling are given by (5) & (6)-

$$\frac{d}{dt} i_d = \omega^* i_q + \frac{1}{L} (u_d - v_d) \quad (5)$$

$$\frac{d}{dt} i_q = -\omega^* i_d + \frac{1}{L} (u_q - v_q) \quad (6)$$

The capacitor voltage can be written similarly in the dq reference frame including cross coupling as shown in (7) & (8)-

$$\frac{d}{dt} v_d = \omega^* v_q + \frac{1}{C} \left(i_d^* - \frac{v_d}{R} \right) \quad (7)$$

$$\frac{d}{dt} v_q = -\omega^* v_d + \frac{1}{C} \left(i_q^* - \frac{v_q}{R} \right) \quad (8)$$

Both the outer voltage loop and inner current loop are also designed by eliminating cross coupling between d and q axis components. The inner loop regulates the currents such that $i_d(t) = i_d^*(t)$ and $i_q(t) = i_q^*(t)$, by controlling the inverter duty cycles. Equation (1) to (8) represent the mathematical modelling of grid forming inverter controller. The control architecture of grid forming inverter without current/voltage control loop and with current/voltage control loop are shown in Fig. 3.1 & Fig. 3.2. The effectiveness of these two control algorithms have been assessed in this chapter under five different case studies.

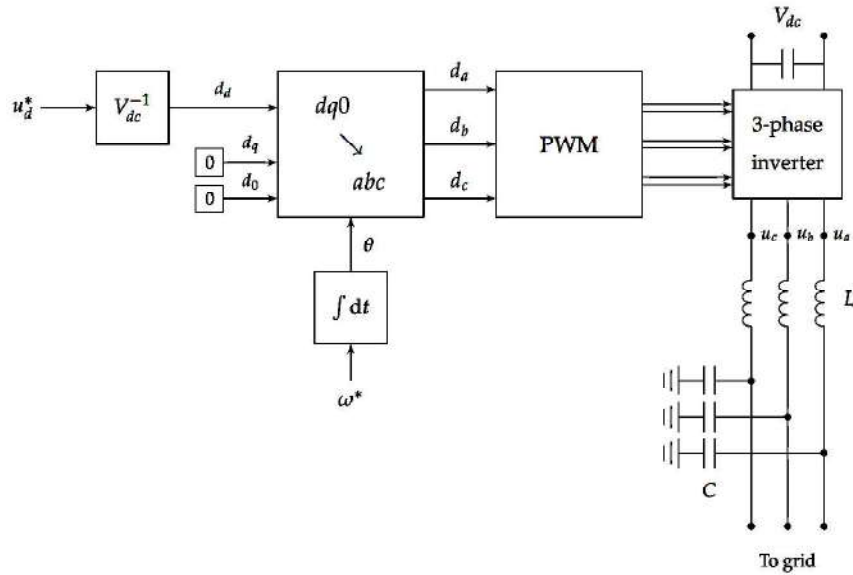


Fig. 3.1. Control Scheme of Grid Forming Inverters (Without current or voltage control loop)

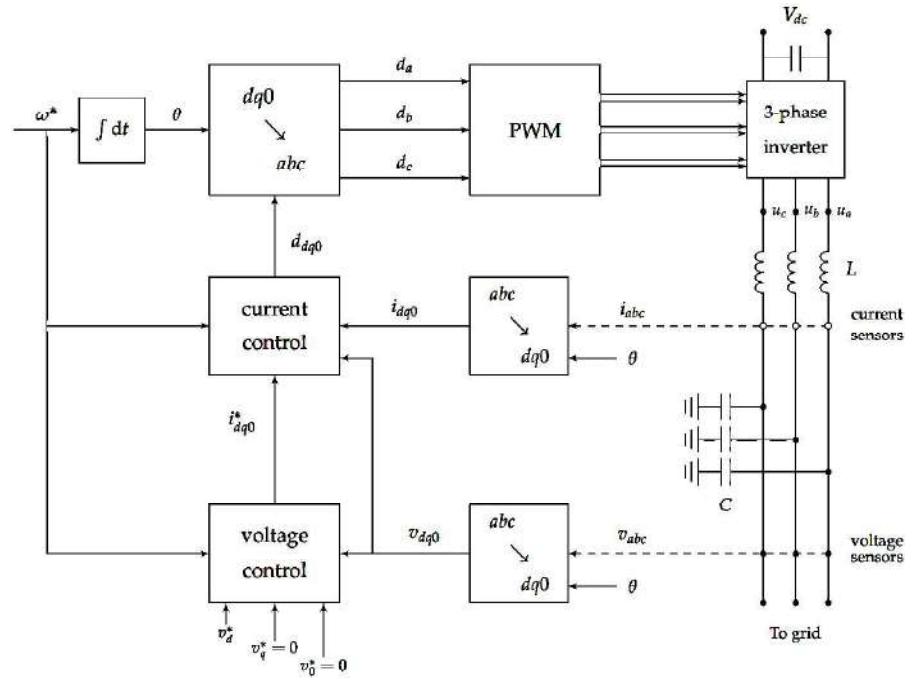


Fig. 3.2. Control Scheme of Grid Forming Inverters (With current or voltage control loop)

3.2 Simulation Setup

The MATLAB/SIMULINK model implementation of the system under study is shown in Fig. 3.3. The parameters used for the designing of the control loops of the inverter are shown in Table 3.1. Grid connected PV system can be both of single stage or multi-stage depending upon the type of applications (see Fig. 3.4). The scheme used for the analysis of this paper is multi-stage PV system i.e. with a DC-DC converter stage with MPPT. The inverter used is a 6 pulse three phase grid forming inverter or voltage source inverter. The inverter is equipped with a dq0 transformation-based controller for controlling the current and voltage injected by the inverter. The inclusion of the current controller and voltage controller in the inverter circuit makes it best suited for both standalone and grid connected applications than the inverter with no current or voltage controller loop.

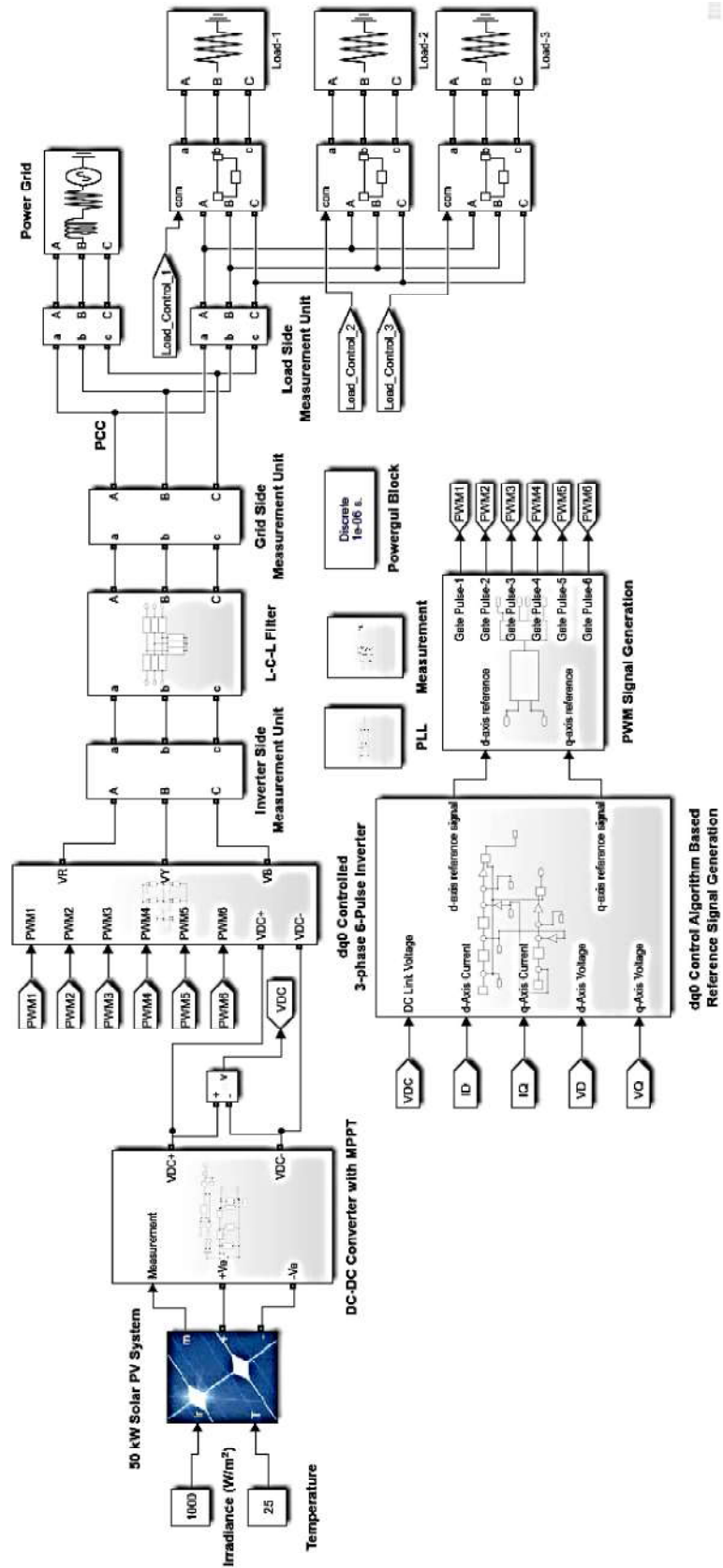


Fig. 3.3. MATLAB/SIMULINK implementation of the grid connected PV system

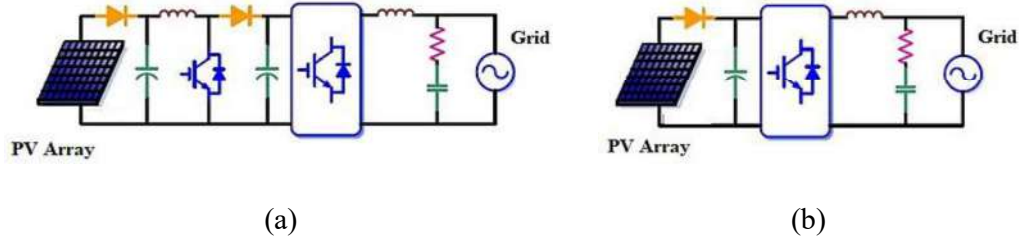


Fig. 3.4. Grid connected PV array (a) multi-stage and (b) single-stage

Sinusoidal pulse width modulation (SPWM) is used for the generation of PWM signal for the inverter gate pulses to get controlled output. PLL is used for initial grid synchronization which gives the frequency and speed of the system as output employing a PI controller. Good approximation of PI controller parameters is necessary for accurate estimation of the system frequency. The voltage control and current control loop used three PI controllers, which process the d and q reference input from the grid voltage and inverter current to generate the output voltage reference for PWM generation.

Table 3.1: Specifications of parameters of the dq0 based grid-forming inverter

Parameter (Symbol)	Value
Inverter type	6-pulse, 3-phase
Nominal grid phase to phase voltage (V_{rms})	400 V
Nominal grid frequency (f_n)	50 Hz
Nominal angular speed (ω_n)	314.16 rad/s
Inverter switching frequency (f_{inv})	10 kHz
Inverter filter inductance (L_{inv})	500 μ H
Inverter filter capacitance (C_{inv})	100 μ F
Inverter internal series resistance of LC elements (R_{inv})	1 m Ω
Load Power (P_{Load})	100 kW
Proportional gain of PLL ($K_{PLL(p)}$)	10 (rad/s)/V
Integral gain of PLL ($K_{PLL(I)}$)	50000 (rad/s)/(V*s)
Proportional gain of PI controller-1 of inverter ($K_{PI-1(p)}$)	0.25 (rad/s)/V
Integral gain of PI controller-1 of inverter ($K_{PI-1(I)}$)	300 (rad/s)/(V*s)
Proportional gain of PI controller-2 of inverter ($K_{PI-2(p)}$)	10 (rad/s)/V
Integral gain of PI controller-2 of inverter ($K_{PI-2(I)}$)	20 (rad/s)/(V*s)
Proportional gain of PI controller-3 of inverter ($K_{PI-3(p)}$)	10 (rad/s)/V
Integral gain of PI controller-3 of inverter ($K_{PI-3(I)}$)	20 (rad/s)/(V*s)

3.3 Case Study and Simulation Results

The performance of dq0 transformation-based grid forming inverter was compared with inverter control without any internal current/voltage control loop through simulation results obtained from MATLAB/SIMULINK model. The simulations were carried out in discrete mode using solver ode23t (mod. stiff/Trapezoidal) setting maximum step size as “auto” and relative tolerance of 1×10^{-3} . The inverter was connected with the grid at PCC where three different resistive loads were also connected with total load demand of 100 kW (Load-1: 50 kW, Load-2: 25 kW and Load-3: 25 kW). The simulation time was set to be 1.0 second. The performance of dq0 based inverter (grid forming) was compared with the inverter with no current or voltage control loop under five different case studies.

3.3.1 Case study-1: Constant irradiance and varying loads

This case study was done keeping the solar irradiance value constant at 1000 W/m^2 and temperature at 25° C . The load connected to the system was varied to see the response of the system for both cases. Load-1 (i.e. 50 kW) was connected at $t = 0.30 \text{ s}$, load-2 (i.e. 25 kW) was added with the system at $t = 0.55 \text{ s}$ and finally load-3 (i.e. 25 kW) was added at $t = 0.80 \text{ s}$. According to the simulation results obtained in Fig. 3.5, the dc link voltage in case of conventional controlled settled to a high value i.e. 1500 V due to the lack of voltage control loop where in case dq0 controlled, the dc link value was seen to be regulated to 600 V as desired and the settling time was also small. The same MPPT algorithm was applied for both cases and hence the outputs were quite same. Depending on the load demand, the utility grid absorbs or deliver power to the PCC. Upto $t = 0.30 \text{ s}$, the load demand was 0 kW and hence the inverter was delivering full power generated by the solar PV to the grid and grid absorbed that power as verified from the output graph. After $t = 0.30 \text{ s}$, as loads were increased step by step, the total demand of the load was shared by the inverter and grid. The simulation results show that, significant power oscillations are present in case of conventional controller where a stable power flow is achieved in case of dq0 controlled grid forming inverter. Power oscillations in the grid power and inverter power is a sign of instability.

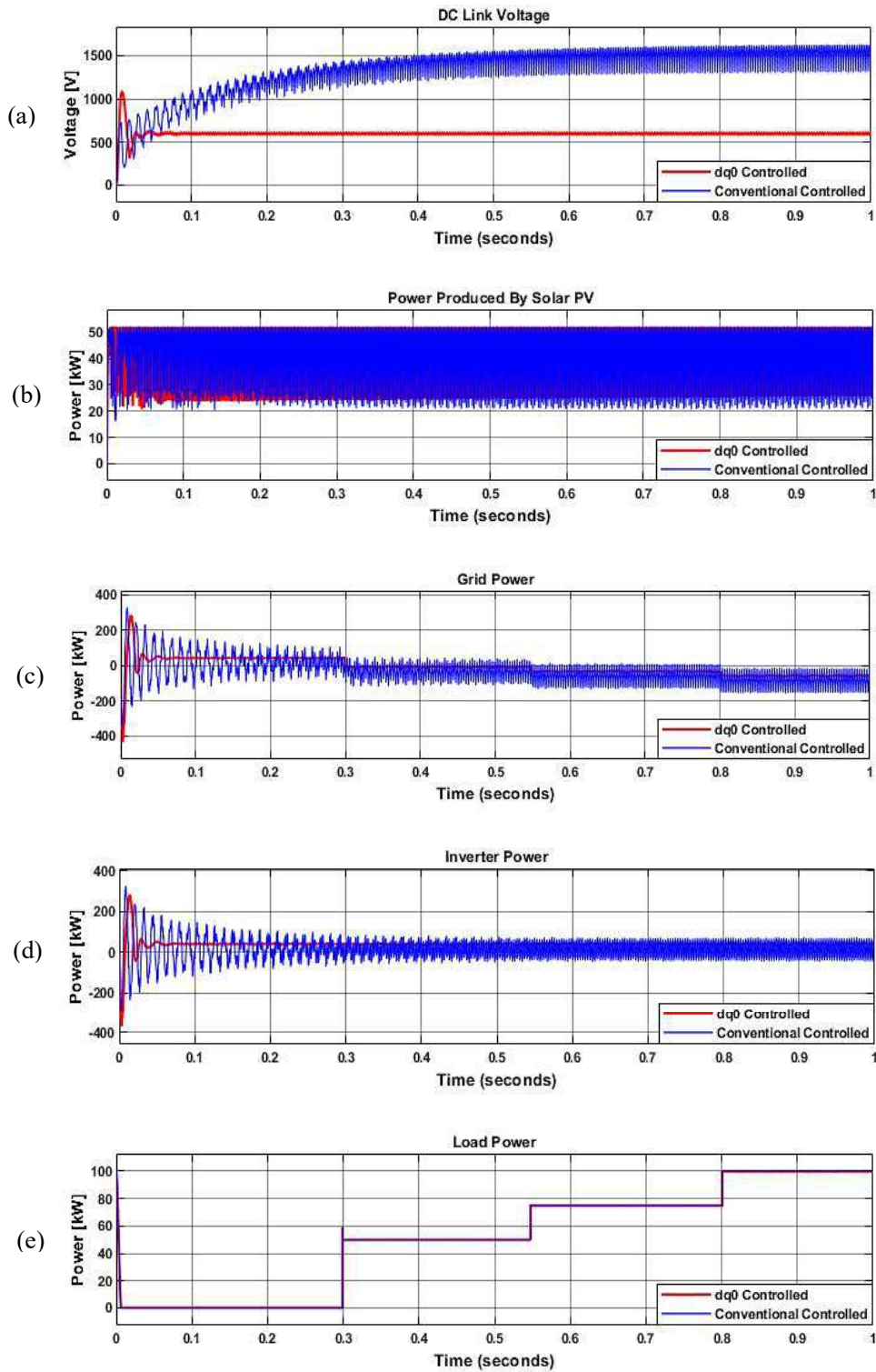


Fig. 3.5. Simulation results for case study-1 (a) DC link voltage at the inverter input (b) Power produced by solar PV array (c) Power absorbed/delivered by the grid (d) Power delivered by the inverter and (e) Load power demand

3.3.2 Case study-2: Dynamic weather condition and constant load

In this section of analysis, a dynamic weather situation has been designed as an input to the PV module to see the response of the system. Varying irradiance of 1000 W/m^2 set as the input from $t = 0 \text{ s}$ to $t = 0.30 \text{ s}$. After that, the irradiance has been changed to 500 W/m^2 at $t = 0.30 \text{ s}$ and again changed to 200 W/m^2 at $t = 0.70 \text{ s}$ as shown in Fig. 3.6. The load connected to the system was set to be 100 kW and was kept constant during whole analysis.

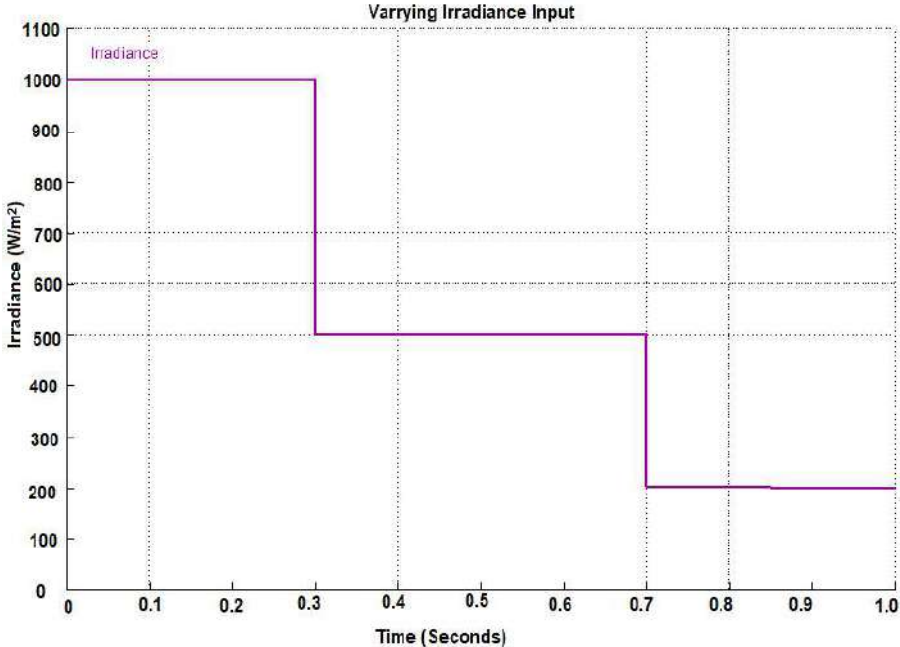


Fig. 3.6. Varying irradiance (W/m^2) at the input of solar PV module

The simulation results show that the MPPT is working fine to extract maximum power from the PV array as determined by the P-V graph for varying irradiance. The system responses with dynamic weather situation are shown in Fig. 3.7. The dc link voltage was observed to be varied with the irradiance level for conventional controlled whereas the voltage was maintained at 600 V by the operation of voltage control loop irrespective of the irradiance level or weather condition. The simulation outputs showed that the power delivered by the grid and inverter changes with the change of irradiance. The grid power increased as the inverter output decreased to meet the total load demand which was set to 100 kW . Significant oscillations in the grid and inverter power were observed for conventional control where dq0 controlled grid-forming inverter showed improved response to the varying inputs to the system.

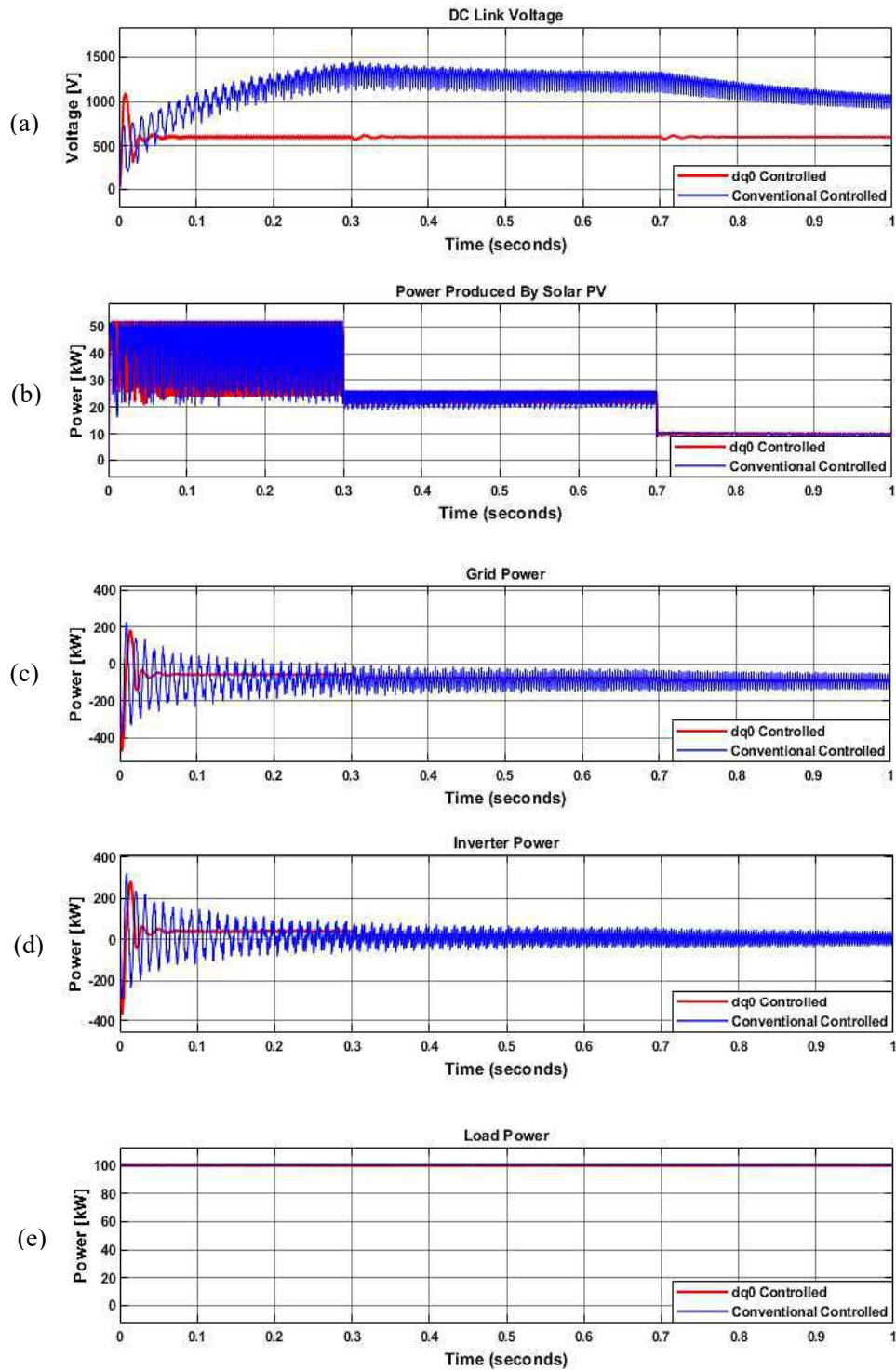


Fig. 3.7. Simulation results for case study-2 (a) DC link voltage at the inverter input (b) Power produced by solar PV array (c) Power absorbed/delivered by the grid (d) Power delivered by the inverter and (e) Load power demand

3.3.3 Case study-3: Back-to-back three phase fault at point of common coupling (PCC)

In this part of analysis, a back-to-back 3 phase transient short circuit fault was created at the point of common coupling (PCC) to see the response of the system. The first stroke of the fault was applied from $t = 0.30 \text{ s}$ to $t = 0.38 \text{ s}$ (i.e. for 0.08 seconds) and the second stroke was applied from $t = 0.63 \text{ s}$ to $t = 0.72 \text{ s}$ (i.e. for 0.09 seconds).

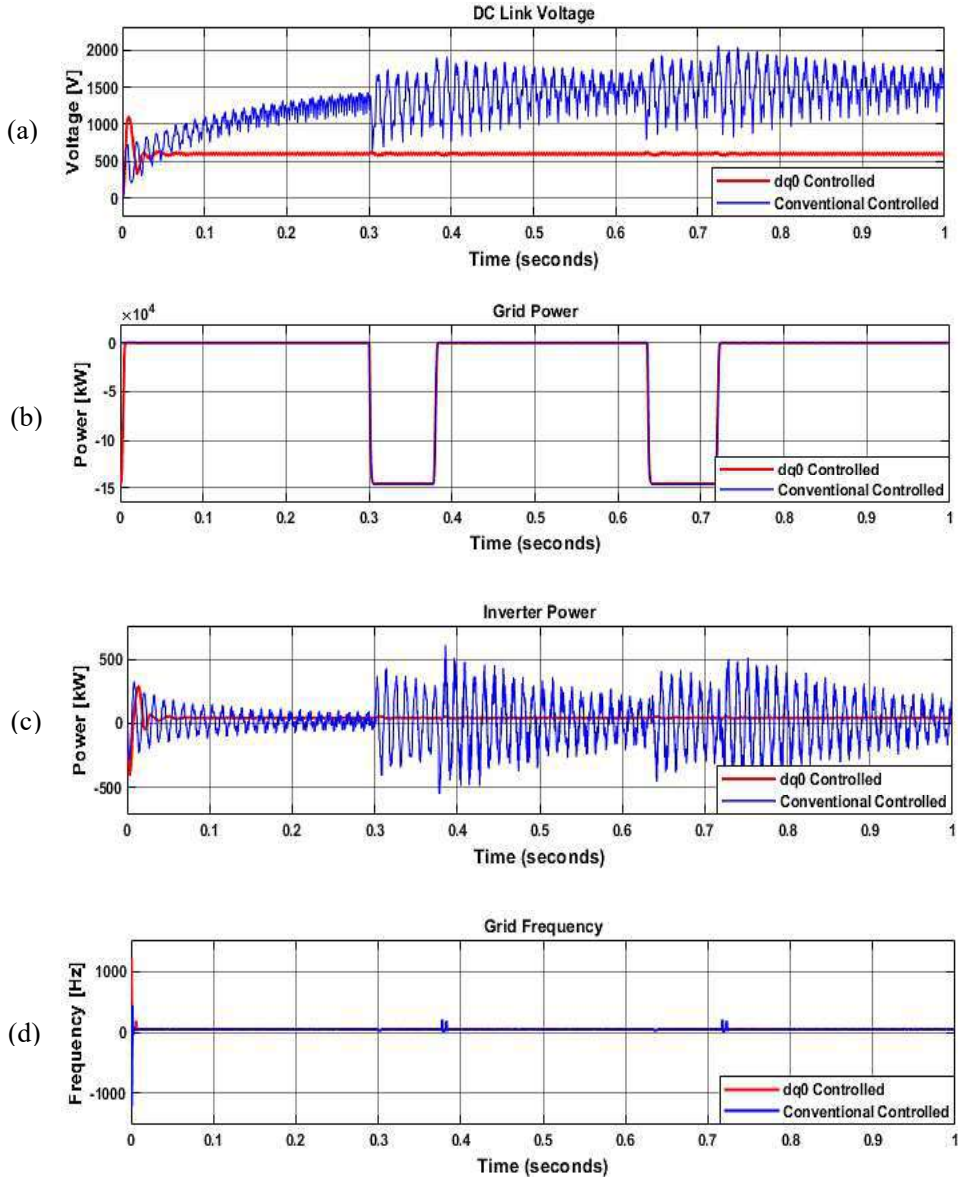


Fig. 3.8. Simulation results for case study-3 (a) DC link voltage at the inverter input (b) Power absorbed/delivered by the grid (c) Power delivered by the inverter and (d) Frequency of the grid at PCC

High oscillations in the dc link voltage was observed in case of conventional control where in case of dq0 controlled based inverter, the dc link voltage stabilized after few moments to 600 V as shown in Fig. 3.8. The grid delivers huge amount of real power to the fault point as seen from the graph. Severe power oscillations was noticed for conventional control where the inverter power with dq0 control settled so rapidly to retain stability of the system. The three-phase fault affects grid frequency severely for conventional cases whereas dq0 controller-based inverter showed better performance and quick recovery of the system frequency.

3.3.4 Case study-4: Three phase short circuit fault at the inverter side

In this case study, a three-phase short circuit fault was applied at the inverter side i.e. before LCL filter at $t = 0.30$ s and the fault was removed at $t = 0.40$ s. The dc link voltage dropped to zero immediately after the occurrence of the fault and the overshoot of the dc link voltage after fault clearance was found to be higher i.e. 5 kV for dq0 control based inverter and higher settling time for conventional control based inverter was noticed. The corresponding grid power and inverter power is shown in Fig. 3.9 where severe oscillations were observed for conventional control inverter and higher overshoot for dq0 based inverter with minimum settling time. The grid frequency was recorded to be severely affected by this fault and the nature of the frequency variation for both cases are oscillatory in nature. The frequency nadir after the fault was recorded as 47.8 Hz for conventional control-based inverter whereas the frequency nadir for dq0 controlled inverter was recorded to be 49.2 Hz. Moreover, an improvement of ROCOF by at least 0.45% was observed for grid forming inverter than conventional inverter.

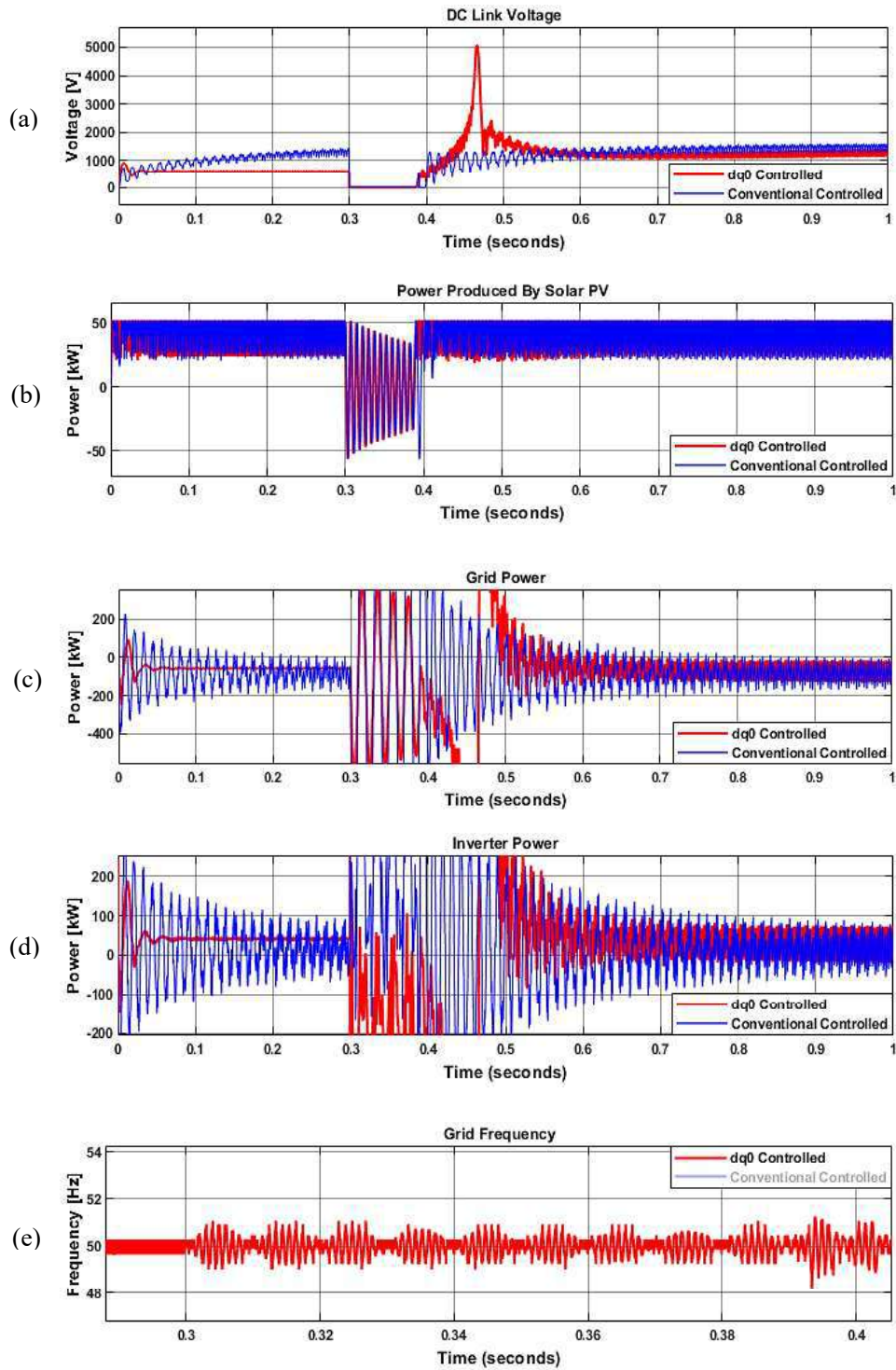


Fig. 3.9. Simulation results for case study-4 (a) DC link voltage at the inverter input (b) Power produced by solar PV array (c) Power absorbed/delivered by the grid (d) Power delivered by the inverter (e) Grid frequency for dq0 Controlled

3.3.5 Case study-5: Short circuit fault on the dc link capacitor side

There is very few research to study the effects of faults on the dc side on the grid for a grid connected PV system. Therefore, in this section, the effects of pole-to-pole fault at the terminal of dc link capacitor has been studied in details to characterize the effects of this type of fault on the system i.e. grid and also after several simulations, authors have tried to identify the stability limit for this case to have a concluding remarks. In this section of case study, two different situations have been studied by varying the fault clearing time to identify the critical clearing time (CCT) for the studied system to ensure stability and reliability of the system. Throughout the simulation study, all the three loads were connected to the system i.e. 100 kW.

3.3.5.1 Fault applied for 0.05 seconds (from 0.30 s to 0.35 s)

In this case, the pole-to-pole dc fault has been created at $t = 0.30$ s and the fault was cleared at $t = 0.35$ s to see the response of the system. So, the fault was applied for a time period of 0.05 seconds. The simulation results obtained from the analysis showed that the dc link voltage goes immediately to zero and the PV array generated power reaches to zero after few oscillations as shown in Fig. 3.10. The total demand of the load (i.e. 100 kW) connected to the system was fulfilled by the grid since the power output of the inverter is also zero. Although the fault has been removed from the dc link capacitor after 0.05 s, the system remains in its previous state and hence the DC side becomes non-functional or the system can be said to unstable. This sudden disconnection of the PV from the system creates oscillation to the system frequency and the oscillations are severe for conventional case than that of dq0 controlled case. Hence from the study of this section, it has been seen that the system becomes unstable for both cases.

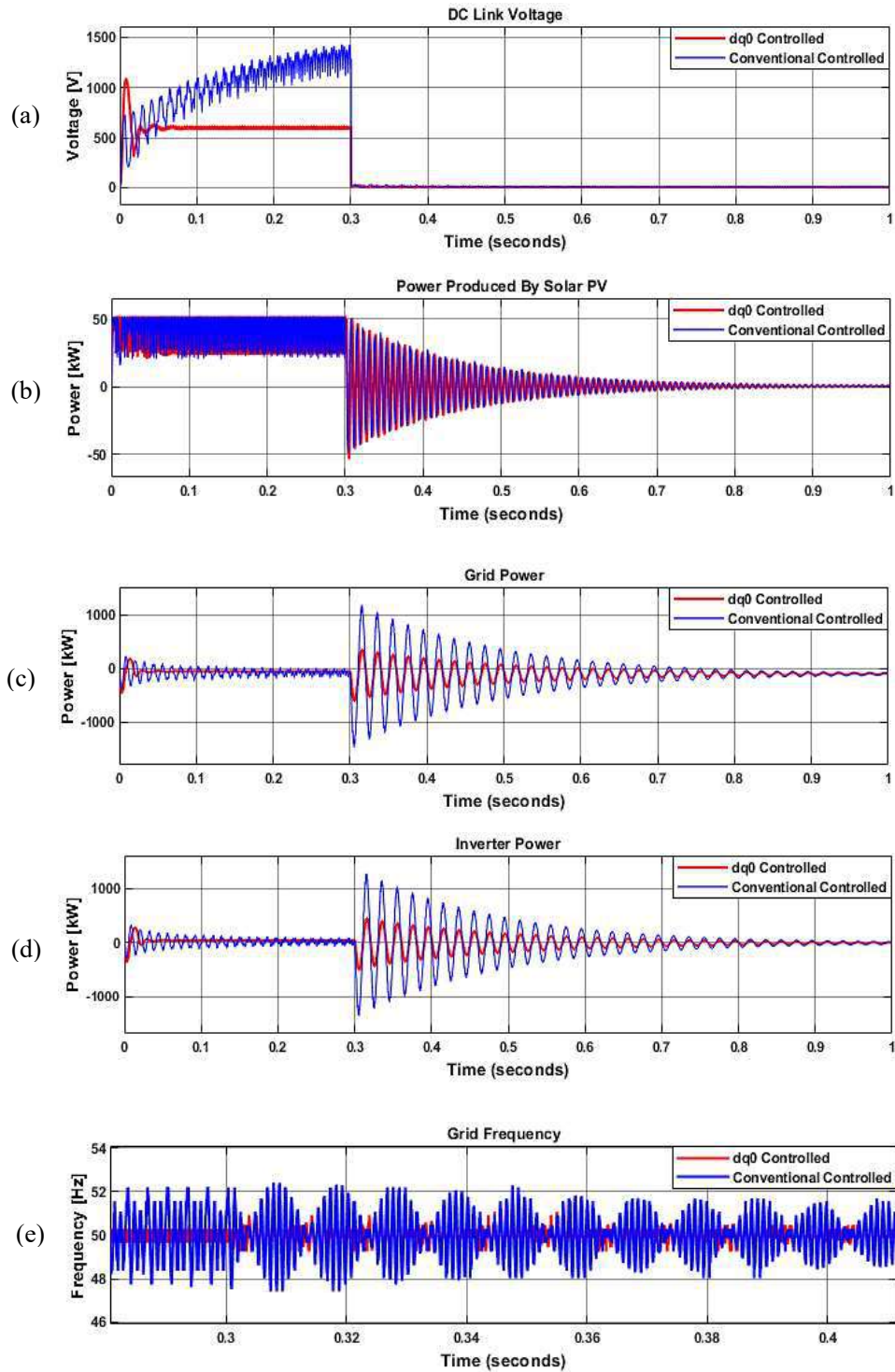


Fig. 3.10. Simulation results for case study-3 (a) DC link voltage at the inverter input (b) Power produced by solar PV array (c) Power absorbed/delivered by the grid (d) Power delivered by the inverter and (e) Frequency of the grid at PCC

3.3.5.2 Fault applied for 0.02 seconds (from 0.30 s to 0.32 s)

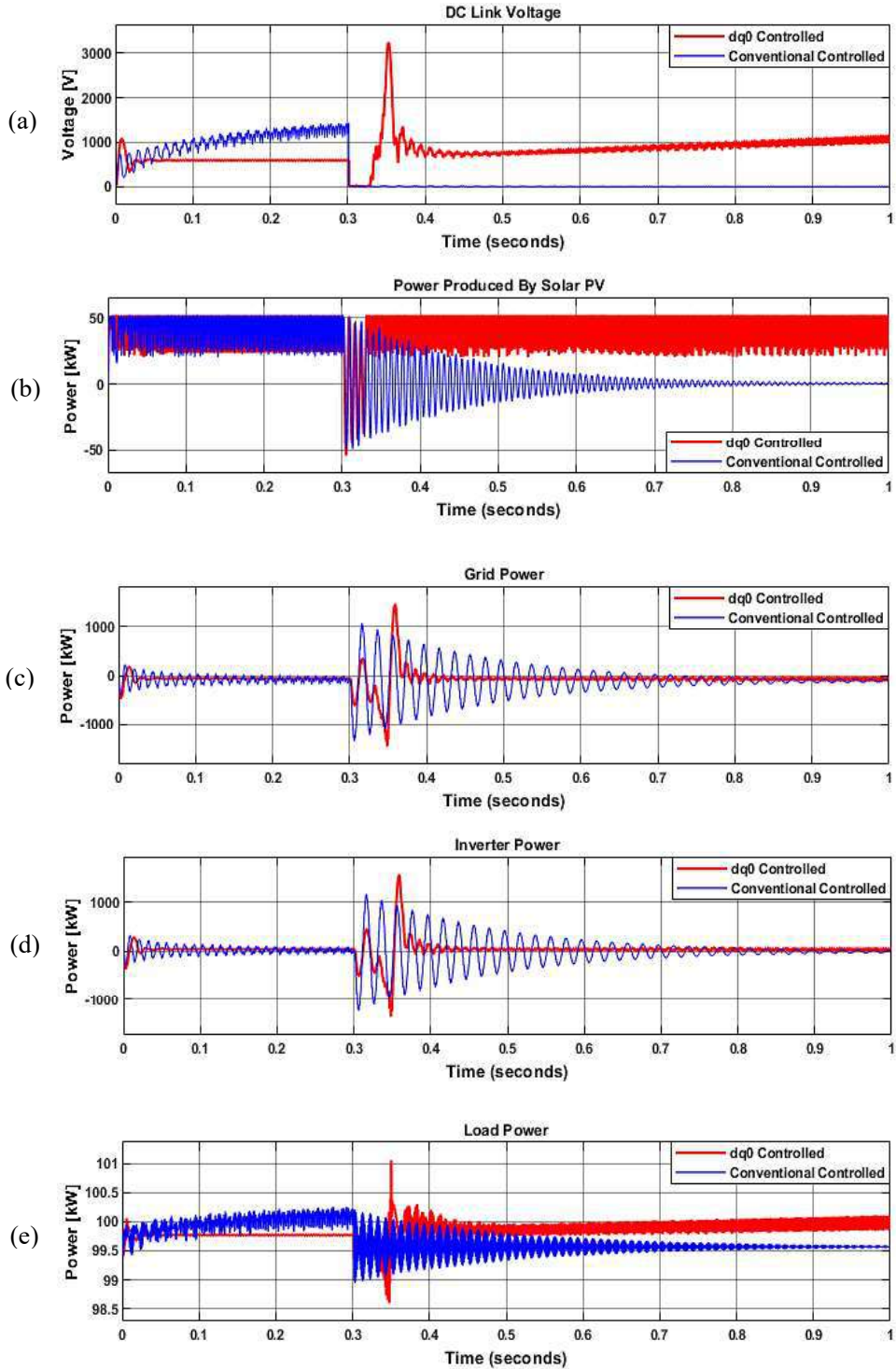


Fig. 3.11. Simulation results for case study-3 (a) DC link voltage at the inverter input (b) Power produced by solar PV array (c) Power absorbed/delivered by the grid (d) Power delivered by the inverter and (e) Load power demand

Several simulations have been done to find the stability limit in terms of CCT and authors have found that a pole-to-pole DC short circuit fault at the DC link capacitor for a duration of 0.02 seconds is the maximum allowable time for fault clearance. Hence to justify the observation, a pole-to-pole short circuit fault was injected across the dc link capacitor starting from $t = 0.30\text{ s}$ to $t = 0.32\text{ s}$. The simulation results showed that, the conventional controlled inverter was unable to get back to stable operation whereas the dq0 controlled grid-forming inverter showed stable operation after few oscillations. The simulation outputs are shown in Fig. 3.11 where it is observed that the conventional controlled inverter is unstable.

3.4 Discussions

An extensive analysis and comparison between conventional grid-connected inverter (i.e. without any voltage or current control loop) and dq0 control based grid forming inverter is presented based on five different case studies. The simulation results obtained from MATLAB/SIMULINK model verified that the dq0 transformation-based grid-forming inverter having both current and voltage control performs better than the conventional inverter without any control mechanism in terms of transient response, frequency nadir, ROCOF and power oscillation reduction. As a result of the superior performance of the modified DQ0 control algorithm-based grid forming inverter with voltage and current control loop, this controller has been utilized for designing the inverter controller for a grid connected BESS system. The detailed designing of the BESS controller has been presented in chapter 4.

Chapter-4

Adaptive Battery Energy Storage System Controller Design

4.1 Proposed Adaptive Fuzzy-ANFIS Hybrid Controller

The system configuration taken into consideration in this research is depicted in Fig. 4.1, where the BESS is linked to the grid at the PCC using a DC-DC bidirectional converter, an inverter, and an LCL filter. The DC-DC converter enables two-way power flow, while the inverter converts the DC input from the BESS to AC and the filter after the inverter lowers the harmonics content. Since the system is solely intended for frequency support, the BESS can only supply a maximum of 10 kW of active power, and it contributes essentially no reactive power. The grid frequency was 50 Hz, and a load of 20 kW was connected at PCC. To regulate the operation of the BESS and inverter, two distinct control units have been created. This section covers the in-depth modelling of the ANFIS system and FLC that the authors of this paper have proposed.

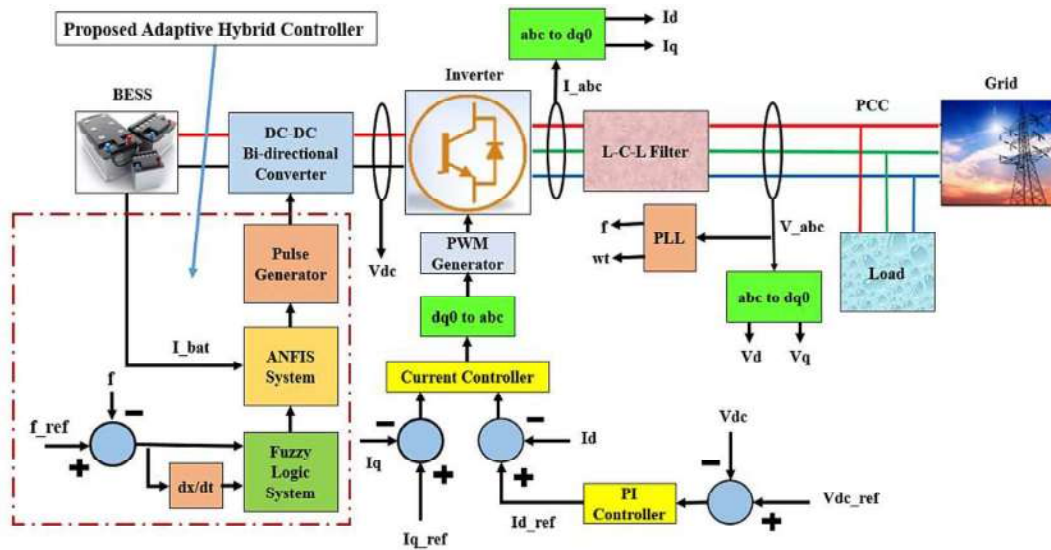


Fig. 4.1. System configuration of the proposed system connected to a low inertia grid.

4.1.1 Fuzzy logic Inference System Design

Due to its high convergence, imprecise input, etc., FLCs are artificial decision-making controllers that are frequently utilized in current control systems. It goes through three stages: defuzzification, rule basis design, and fuzzification. The designer should have prior experience with the test system when defining the rules in order to implement the FLC. During the fuzzification process, the crisp input variables are transformed into fuzzified values using the Mamdani method in accordance with membership functions (MFs).

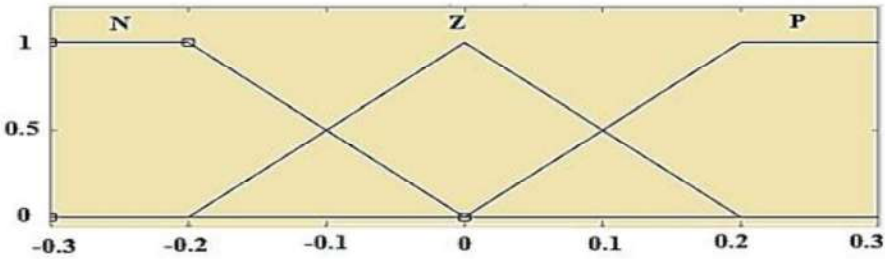


Fig. 4.2. Membership functions plot of input variable (Frequency Error)

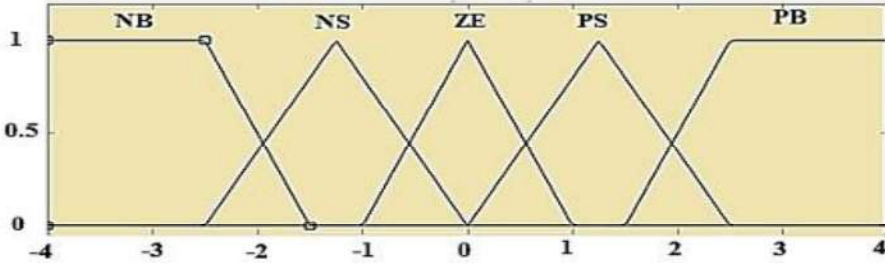


Fig. 4.3. Membership functions plot of input variable (ROCOF)

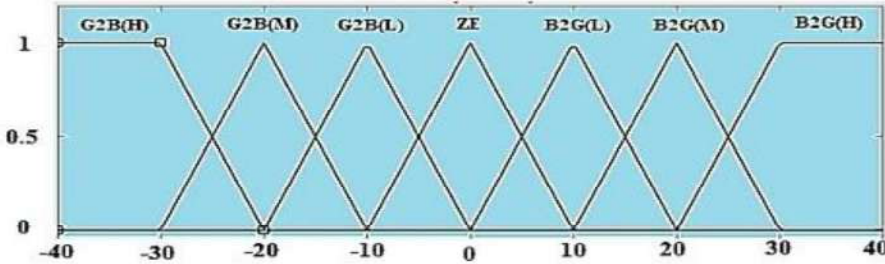


Fig. 4.4. Membership function plot of output variable (Adaptive Current Reference)

A suitable fuzzy output is then produced using fuzzy rules once the fuzzy set has been analysed in the inference system. Following that, the fuzzy output is transformed into a systematic crisp value as a form of duty cycle in defuzzification. Defuzzification is accomplished via the centroid approach. First-stage FLC, which has two inputs and one output, is used in the design of the BESS controller. The frequency error and ROCOF are used as the inputs, and the BESS current reference is used as the output for creating pulses. Triangular MFs, as depicted in Fig. 4.2 to Fig. 4.4, is used to design the inputs and outputs. There are three membership functions for first input (i.e. frequency error) like N (Negative), Z (Zero) and P (Positive) and it ranges from -0.30 to +0.30. For second input (i.e. ROCOF), the number of membership functions are five and they are NB (Negative Big), NS (Negative Small), ZE (Zero), PS (Positive Small) and PB (Positive Big). The range for this input is from -4.0 to +4.0.

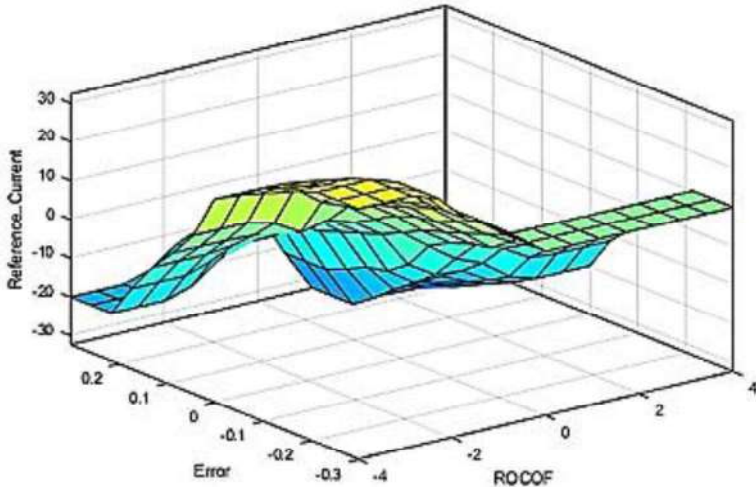


Fig. 4.5. Three-dimensional surface plot of fuzzy inference system rules

The output variable has also seven MFs namely G2B(H), G2B(M), G2B(L), ZE, B2G(L), B2G(M) and B2G(H) where G2B stands for grid to BESS, B2G stands for BESS to grid, ZE stands for Zero and H, M and L stand for High, Medium and Low respectively. The output of FLC is the adaptive current reference that ranges from -40 to +40. The three-dimensional plot of the rules is shown in Fig. 4.5. The rules have been designed based on the above mentioned MFs as shown in Fig. 4.6.

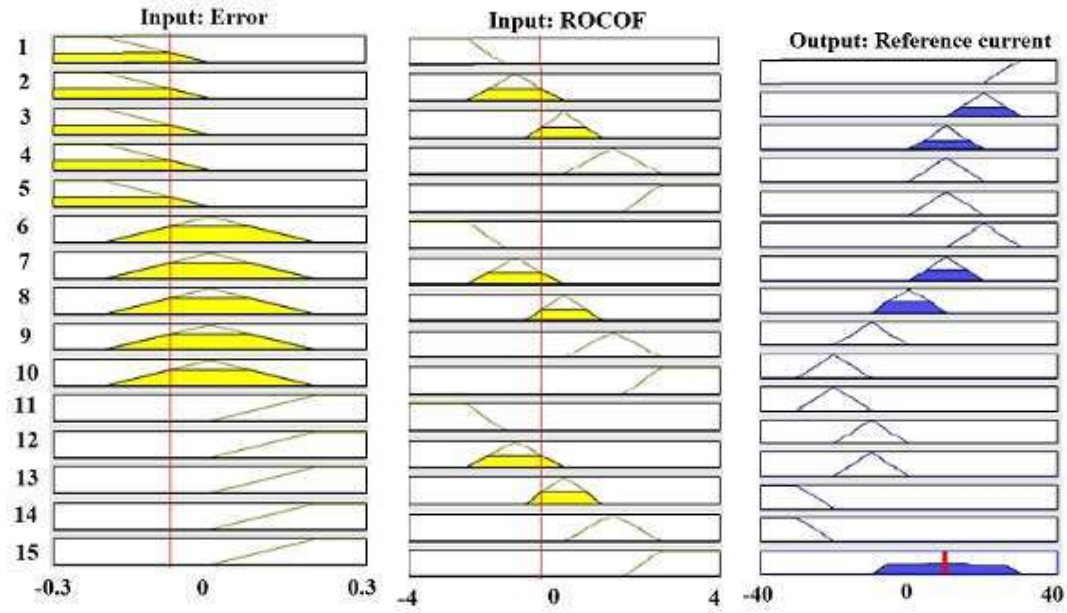


Fig. 4.6. Rules viewer of fuzzy logic inference system

The rules are so designed that the current reference will change adaptively based on the value of frequency error and ROCOF. The system is built to produce a control signal for BESS in the event of a large error value and ROCOF, allowing for speedy power delivery and absorption to lower frequency deviation. The power delivered/absorbed is regulated adaptively based on the changes in the input values and hence this feature of the proposed controller helps to outperform under any abnormalities.

Table 4.1: Fuzzy rules used for proposed controller

Input-1: Frequency Error (e)	Input-2: Rate of change of frequency (ROCOF)				
	NB	NS	ZE	PS	PB
N	B2G (H)	B2G (M)	B2G (L)	B2G (L)	B2G (L)
Z	B2G (M)	B2G (L)	ZE	G2B (L)	G2B (M)
P	G2B (M)	G2B (L)	G2B (L)	G2B (H)	G2B (H)

When the frequency error/deviation and ROCOF becomes zero simultaneously, the BESS goes to disconnected mode i.e. no power transfer between BESS and grid. Most of the time, the BESS remains in disconnected mode and it activates its power transfer under any abnormal situation. Moreover, the battery is automatically connected to the grid for charging if the SOC of the battery becomes less than 20%. The detailed rules for the FLC system depending on the inputs are shown in Table 4.1.

4.1.2 Adaptive Neuro-Fuzzy Inference System (ANFIS) Design

PI controller is widely used for designing BESS controller for grid support due to its simplicity in operation, cost and flexibility in tuning its different parameters to extract better performance. But due to the slower response of the PI controller and difficulties in selecting exact controller constants value for getting desired response, ANFIS model-based controller are now widely been used in the area of control engineering as well as in designing controllers for RE integration into the grid. Moreover, the performance of PI controller-based BESS controller degrades during large transient event since the parameters of the controller are fixed but not adaptable.

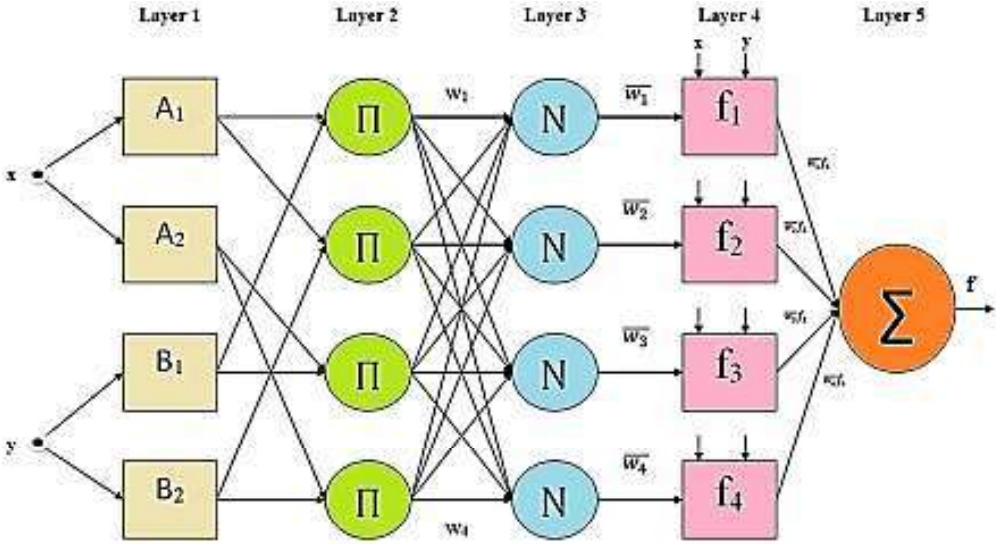


Fig. 4.7. Basic structure of ANFIS model for two inputs

In this part of analysis, the conventional PI controller is replaced by ANFIS model in cascade with fuzzy logic controller that eliminates all the limitations of the BESS controller for providing inertia to the grid to enhance frequency stability. The basic structure of the ANFIS model for two inputs is shown in Fig. 4.7 [64]. From the figure, it is seen that the ANFIS structure consists of five layers. The first layer is the fuzzification layer where the membership degree of each membership functions is calculated using equation (9) and (10).

$$\mu A_i(x) = gbellmf(x; a, b, c) = \frac{1}{1 + \left| \frac{x-c}{a} \right|^{2b}} \quad (9)$$

$$O_i^1 = \mu A_i(x) \quad (10)$$

The second layer is the rule layer where the firing strengths (w_i) for the rules are generated by using membership values computed in layer 1. The firing strengths are manipulated as in (11).

$$O_i^2 = w_i = \mu A_i(x) \cdot \mu B_i(y) \quad ; \text{where } i = 1, 2, \dots, 10 \quad (11)$$

In the third layer, normalization is done where normalized firing strengths are calculated which can be calculated as equation (12).

$$O_i^3 = \bar{w}_i = \frac{w_i}{w_1 + w_2 + w_3 + w_4} \quad ; i \in \{1, 2, \dots, 10\} \quad (12)$$

The fourth layer is the defuzzification layer followed by summation layer as the last one. Weighted values of rules are calculated in each node of defuzzification layer by (13) and the actual output of the ANFIS model is obtained by (14) as follows-

$$O_i^4 = \bar{w}_i f_i = \bar{w}_i (p_i x + q_i y + r_i) \quad (13)$$

$$O_i^5 = \sum_i \bar{w}_i f_i = \frac{\sum_i w_i f_i}{\sum_i w_i} \quad (14)$$

The training data of the input and output were extracted from the Matlab/Simulink model using conventional PI controller and the ANFIS model were trained with the data using hybrid model for 50 epochs. The rules viewer and surface plot of the rules for ANFIS model are shown in Fig. 4.8 respectively.

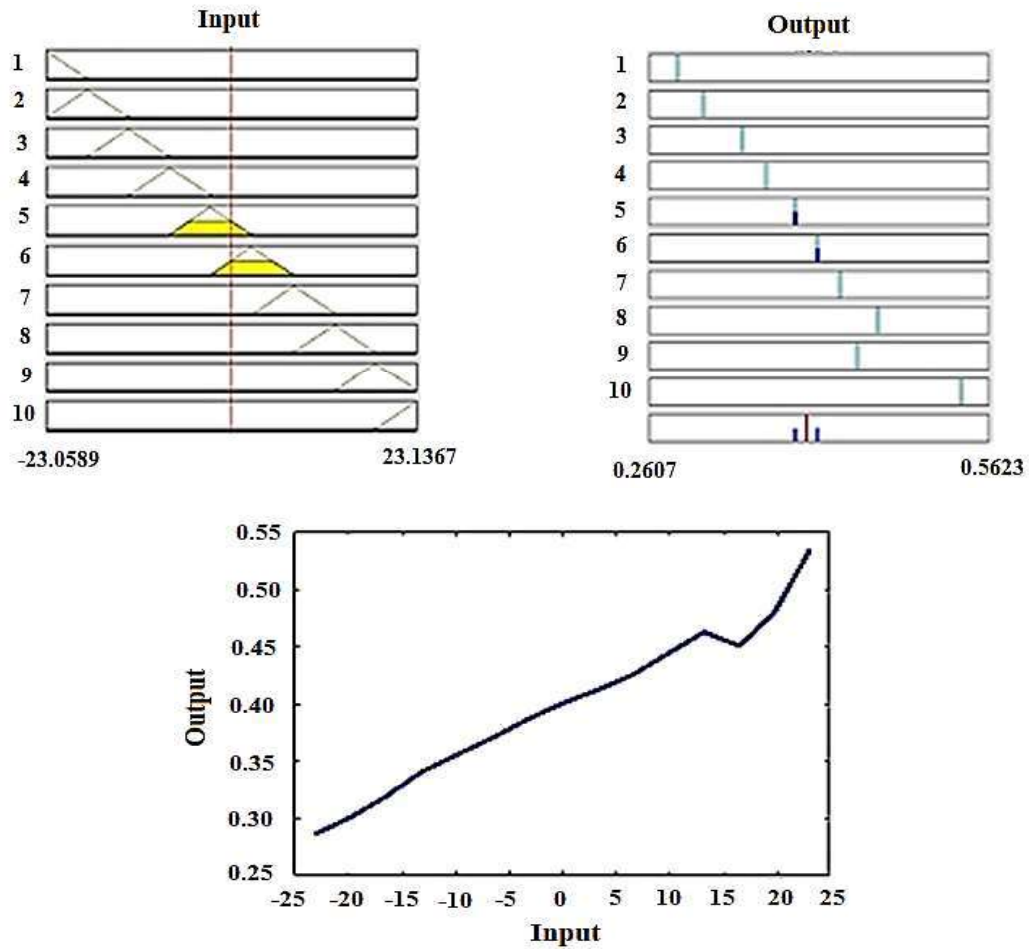


Fig. 4.8. Rules viewer and surface view plot of the ANFIS model

4.2 Components Model and Specifications

4.2.1 Battery Energy Storage System (BESS)

Due to cost reductions, particularly as a result of lithium-ion battery technological advancements, BESS are commonly employed for microgrid applications. In addition to this, lead acid batteries, supercapacitors, sodium sulfide (NaS), ultracapacitors, and other devices are frequently utilized for inertial grid support in a low inertia grid made up of substantial renewable energy sources. Due to its superior benefits, such as lengthy lifecycles, higher energy densities, improved reliability, and low self-discharging rates, Li-ion batteries are widely utilized today, particularly for EV, BESS, etc. [65]-[69]. Additionally, Li-ion batteries are cheaper, more environmentally friendly, and have no memory effect, according to [70], [71].

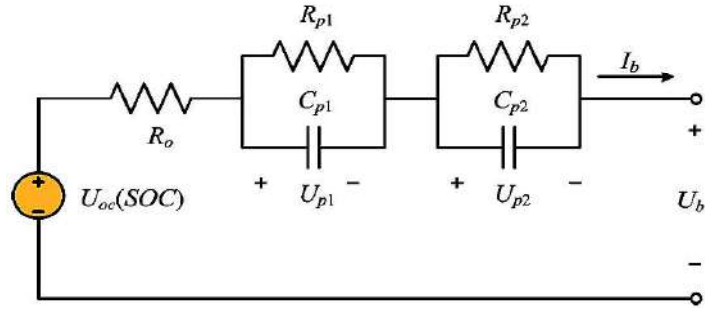


Fig. 4.9. Typical diagram of a battery equivalent circuit model.

The specifications of the Li-ion battery used as BESS for simulation are shown in Table 4.2. Proper mathematical modeling is required to comprehend a battery's internal dynamics and for effective BMS modeling [70], [71]. Empirical models, electrochemical models (also known as physics-based models), and simplified equivalent circuit models can all be used to represent batteries in general [72]. Fig. 4.9 depicts a common framework for a battery equivalent circuit model [65], [66], [73]. In Fig. 4.10, the Li-ion battery under investigation's nominal discharge characteristics is displayed.

Although the BMS prevents the battery from being undercharged or overcharged, the graph shows that it takes roughly 2.3 hours for SOC to reach 0% for a nominal discharging current of 86.96A. The pink-colored shaded area represents the battery's normal functioning region. The characteristics of the battery's discharge for different values of discharging current, such as 6.5A, 13A, and 32.5A, are also displayed. It is clear that the time required for charging and discharging of the battery fully depends on the reference current for charging or discharging the BESS. Therefore, adjustments in the BESS reference current have been made in this article to regulate the battery's charging or discharging rate for inertial grid support.

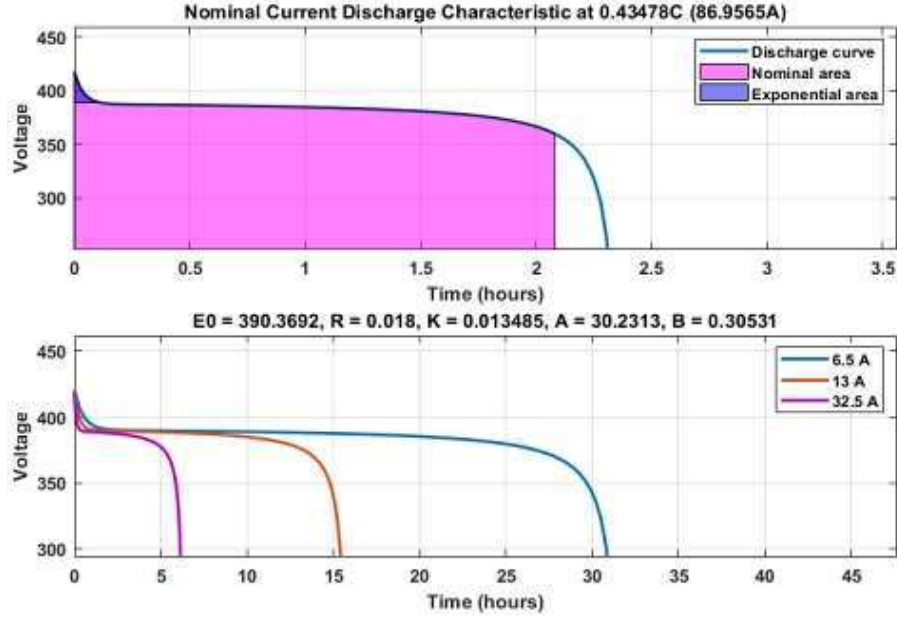


Fig. 4.10. Nominal discharge characteristics plot of the Battery.

4.2.2 Bi-directional Converter and Inverter

DC-DC bi-directional converter is basically a buck-boost converter that can allow both directional power flow and hence it is used for many applications like EVs, uninterruptible power supply (UPS), RESs, BESS applications for both standalone and grid connected mode [74]. Depending on the input signal, the power electronic switches (S1 and S2) of the bi-directional converter (see Fig. 4.11) alternately switch the charging and discharging modes of a grid-connected BESS. Traditionally PI controller followed by a limiter is used to generate the corresponding duty cycle for switching ON/OFF the MOSFETs. The filter inductance and capacitance of the converter have been calculated as 19.8 mH and 300 μ F by the equations (15) & (16):

$$L_F = \frac{V_{Batt} \times (V_{Inv} - V_{Batt})}{I_T \times F_{sw} \times V_{Inv}} \quad (15)$$

$$C_F = \frac{I_r}{8 \times F_{sw} \times V_r} \quad (16)$$

The voltage of BESS at the filter side of the bi-directional converter was 360V where the DC link voltage at the inverter side of the bi-directional converter was set to be 800V. A PI controller has been implemented to control the DC link voltage at its nominal value under any abnormalities.

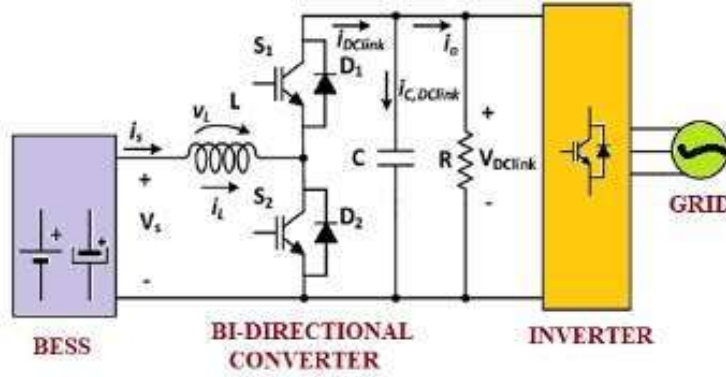


Fig. 4.11. Grid connected bi-directional converter and inverter.

Table 4.2: Specifications of Battery and Inverter

Battery		Inverter	
Parameters (Symbol)	Value	Parameters (Symbol)	Value
Battery Type	Lithium-Ion	Inverter type	6-pulse, 3-phase
Nominal Voltage	360 V	Nominal grid phase to phase voltage	400 V
Rated Capacity	200 Ah	Nominal inverter grid frequency	50 Hz
Initial State-Of-Charge	50%	Nominal angular speed	314.16 rad/s
Battery Response Time	1s	Inverter switching frequency	10 kHz
Maximum Battery Capacity	200 Ah	Inverter filter inductance	467 mH
Cut-off Voltage	270 V	Inverter filter capacitance	110 mF
Fully Charged Voltage	419.0354 V	Internal series resistance of LC elements	1 mW
Nominal Discharge Current	86.9565 A	Load Power	20 kW
Internal Resistance	18 mΩ	Proportional gain of PLL	15 (rad/s)/V
Capacity at Nominal Voltage	180.8696 Ah	Integral gain of PLL	45000 (rad/s)/(V*s)

The inverter regulates how much actual and reactive power flow. The inverter was employed in grid-forming mode, and the inverter controller was developed using the most popular dq0 transformation approach. Time variable a-b-c reference frames are not used in the majority of RE-based control systems since dq0 displays greater performance under transient and steady state conditions. The reference value for reactive power flow has been set to zero since this paper develops the control algorithm for active power support or frequency support emulating virtual inertia by using BESS. The specifications of the inverter are shown in Table 4.2.

4.3 Software Implementation

The system configuration proposed in Fig. 4.1 was implemented in Matlab/Simulink software for validation of the outperformances of the proposed hybrid controller through simulation outputs. The implemented Matlab/Simulink model is shown in Fig. 4.12 where a Battery Energy Storage System (BESS) has been connected with the low inertia grid through multiple stages of conversion for inertial grid support under dynamic abnormal situations. The BESS is so designed to supply a maximum of 10 kW active power to the grid when necessary and simultaneously can absorb same amount of active power when needed. In this way, BESS provides inertia to the grid and overall inertial response of the grid improves.

The resistive load at PCC is connected through a three-phase circuit breaker which is controlled to make the abnormal conditions of under-frequency i.e. sudden load injection and over-frequency i.e. sudden load rejection. The fault module is also used to control the transient three phase fault at PCC to verify the effectiveness of the proposed controller. The input of the adaptive hybrid controller are frequency error (i.e. $e_f = f_a - f_{ref}$) and ROCOF (i.e. de_f/dt). The internal architecture for extracting the input for fuzzy logic controller and generation of control signal by ANFIS model is shown in Fig. 4.13.

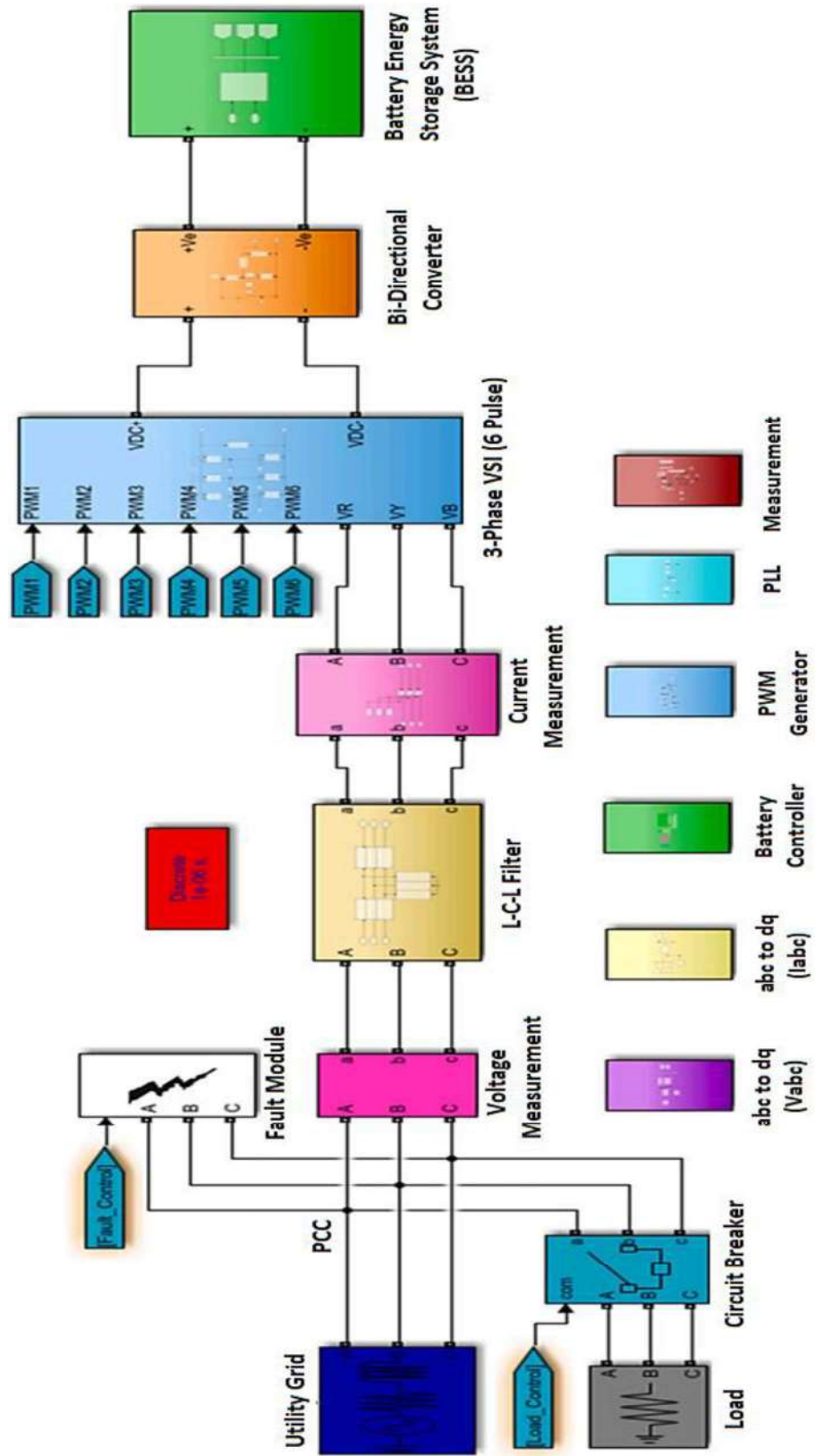


Fig. 4.12. Matlab/Simulink implementation setup of the proposed system

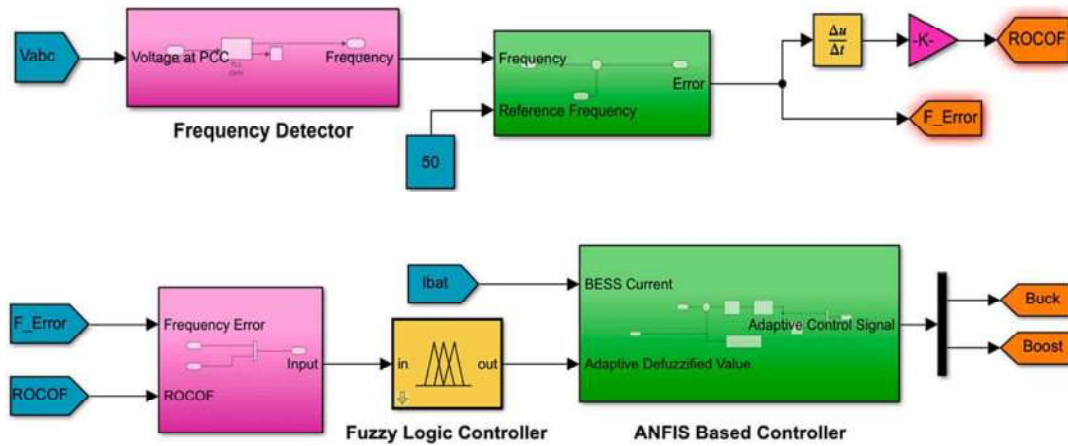


Fig. 4.13. Adaptive hybrid BESS controller implementation in Matlab/Simulink

The frequency of the studies system is detected by a frequency detector (e.g. PLL for this case). The fuzzified output of the FLC is given to the ANFIS controller for generating the control signal for the DC-DC bi-directional converter as shown in Fig. 4.14. The signals ‘Buck’ and ‘Boost’ are fed to the bidirectional converter that controls the state of the battery whether to charge or discharge and hence to control the amount and direction of active power flow from BESS. The controller output is adaptive in nature and hence the direction of active power flow as well as the amount is adaptable based on the value of frequency error and ROCOF.

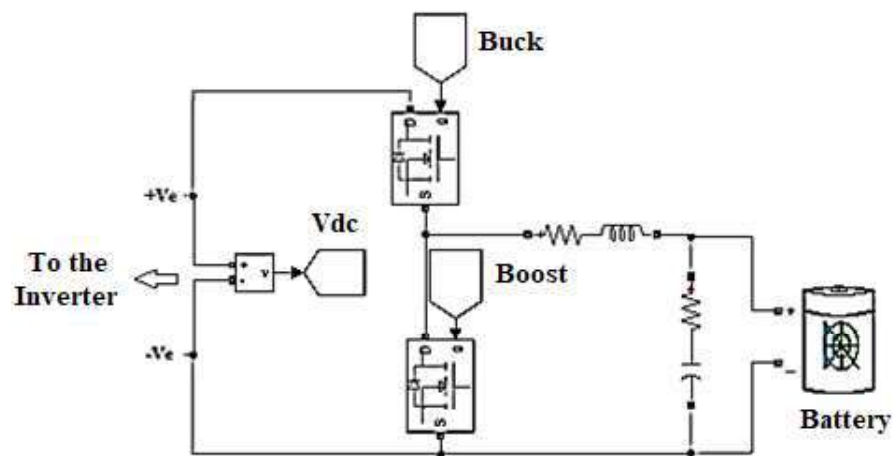


Fig. 4.14. Power flow control of the BESS using DC-DC bidirectional converter.

Chapter-5

Simulation Results and Discussions

5.1 Case Study Sequence

The simulations were carried out in discrete mode using solver ode23t (mod. stiff/Trapezoidal) setting maximum step size as “auto” and relative tolerance of 1×10^{-3} . The effectiveness of the proposed controller was validated by simulation results obtained from different case studies. At the starting of simulation, the network with a BESS utilizing fuzzy logic and PI controller were studied for different abnormalities like under-frequency (i.e. sudden load injection), over-frequency (i.e. sudden load rejection), three phase dead short circuit fault injection and rejection etc. During the study of the base system with FLC-PI controller, the parameters of the PI controller were extracted by using MATLAB/SIMULINK auto-tuning option for PI controller that works based on Particle Swarm Optimization (PSO) technique to get the best system response. The proposed controller has been tested for four different case studies as summarized in Fig. 5.1.

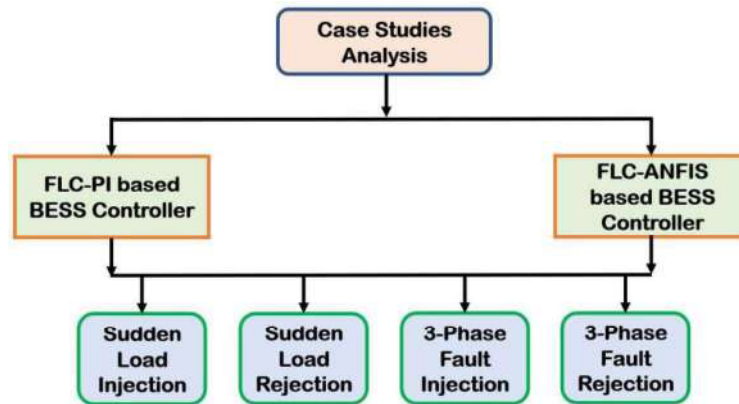


Fig. 5.1. Case study analysis flow diagram

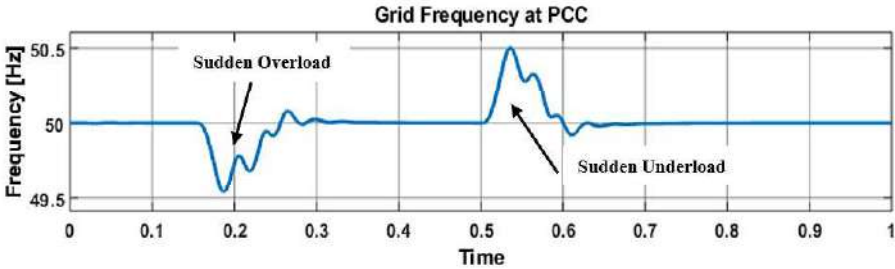
The results for base case (i.e. with a BESS adopting FLC and PI controller) were compared with the proposed case at the end of this section in tabular form to show the effectiveness of the adaptive hybrid algorithm as proposed in this paper. The frequency stability of a low inertia grid can be evaluated based on some important key performance indices (KPIs) like ROCOF, frequency nadir, frequency zenith etc. This paper will

evaluate and compare frequency nadir and ROCOF to show the improvement in frequency stability.

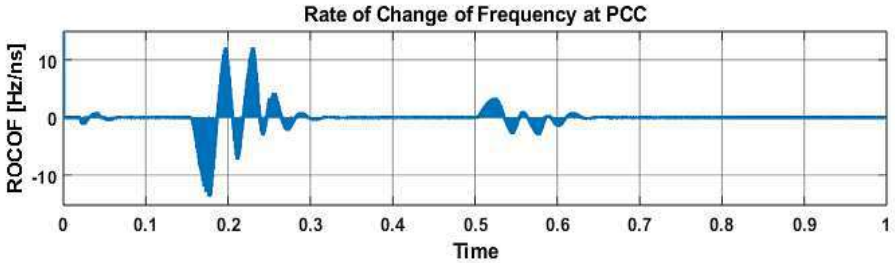
5.2 With a BESS utilizing FLC and PI controller

5.2.1 Sudden load variations (i.e. load injection and rejection) at PCC

In this section of analysis, the system under study was tested for sudden overload and underload at PCC for the designed adaptive fuzzy-PI based BESS controller. The frequency response of the system was observed to evaluate frequency nadir and ROCOF by switching ON and switching OFF the 20 kW load by using a three phase circuit breaker. The sudden overload scenario was done at $t = 0.16$ s by switching ON the circuit breaker using external control. Due to this event, the grid frequency drops significantly due to the low inertia of the grid as shown in Fig. 5.2(a). The frequency nadir was found to be 49.556 Hz and the maximum rise in frequency was 50.113 Hz. After a settling time of 195 ms, the grid frequency stabilizes and returns to its nominal frequency (in this case, 50 Hz).



(a)



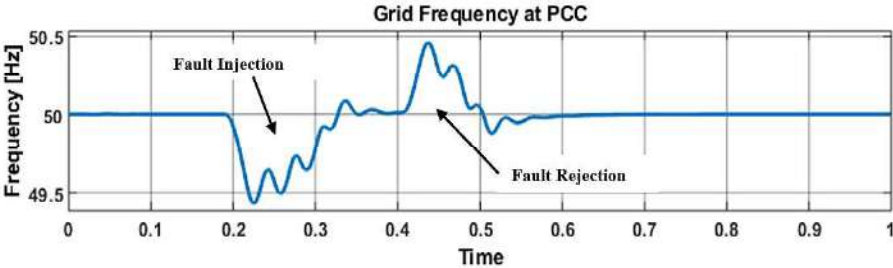
(b)

Fig. 5.2. Sudden load variation (a) Grid frequency at PCC and (b) Rate of change of frequency (ROCOF)

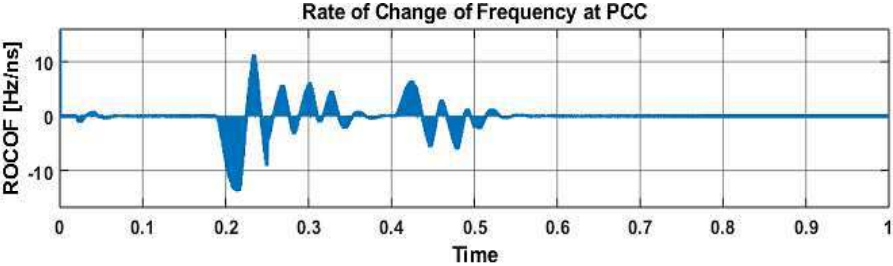
Similarly, to see the maximum rise in frequency of the grid due to underload condition, the connected load at PCC was disconnected at $t = 0.5$ s from the system and it has been observed that the grid frequency increased significantly due to the power imbalance or sudden load rejection for a very short period of time. The maximum frequency overshoot and frequency nadir during this abnormality were found to be 50.512 Hz and 49.863 Hz. The settling time for this case was 170 ms. The ROCOF at PCC was also monitored for both the test case as shown in Fig. 5.2(b). The ROCOF value falls over time as the grid frequency gets closer to its nominal frequency.

5.2.2 Three phase dead short circuit fault at PCC

In this part of analysis, the impact of a three-phase dead short circuit fault injection and rejection were observed. At $t=0.2$ s, the fault was applied, and at $t=0.4$ s, it was removed from the system. According to Fig. 5.3(a), the fault injection resulted in under-frequency and the fault extraction resulted in over-frequency. The corresponding ROCOF recorded at PCC during this event is also shown in Fig. 5.3(b).



(a)



(b)

Fig. 5.3. Three phase short circuit fault (a) Grid frequency at PCC and (b) Rate of change of frequency (ROCOF)

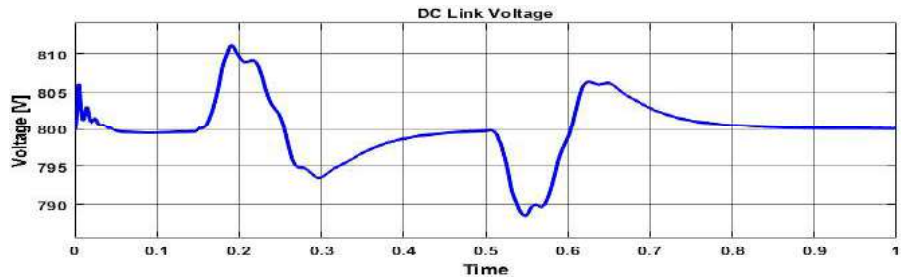
The system's frequency nadir and maximum frequency overshoot were measured to be 49.421 Hz and 50.127 Hz, respectively, after a fault was applied. The minimum frequency and frequency overshoot for fault removal were reported to be 49.807 Hz and 50.451 Hz, respectively. The settling time required for the grid frequency to come to the nominal value were 276 ms and 188 ms respectively.

5.3 BESS with adaptive hybrid controller (FLC-ANFIS) emulating virtual inertia

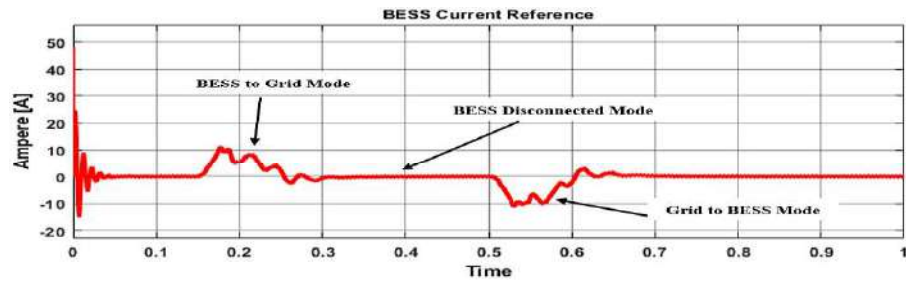
5.3.1 Sudden load variations (i.e. load injection and rejection) at PCC

This part simulates the previously stated system after integrating a Battery Energy Storage System (BESS) with a low inertia grid using the proposed adaptive fuzzy-ANFIS algorithm-based controller to provide inertial support and enhance frequency performance. The same amount of resistive load was suddenly injected to the system at PCC to make the under-frequency event at $t = 0.16$ s and the load was disconnected at $t = 0.5$ s respectively. The simulation results show significant improvements of the frequency response in terms of frequency nadir (i.e. minimum frequency) and ROCOF. From Fig. 5.4, it is seen that the BESS responded instantaneously with the variation of frequency and ROCOF of the grid to minimize the effect of load injection on frequency response. The BESS current reference for active power injection varied adaptively depending on the frequency and ROCOF.

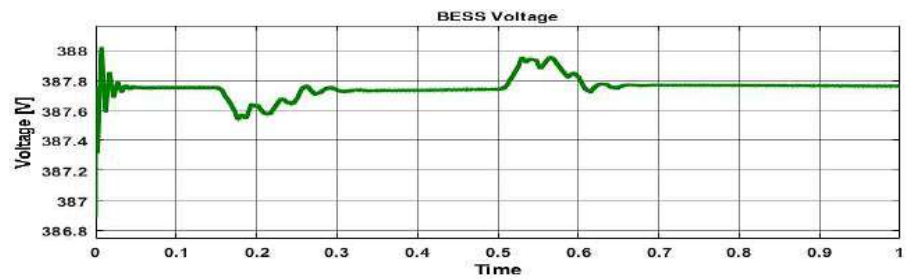
During load injection, the grid frequency falls down and the BESS is connected to the grid automatically by the controller action to supply active power to the grid and the BESS takes active power from the grid during load rejection or over-frequency event. This property of the BESS utilizing the proposed controller enables virtual inertial support to the grid to lessen the value of frequency nadir (Hz) and ROCOF (Hz/ns). The controller ensures constant DC link voltage i.e. 800 V at the inverter side after any abnormal scenarios.



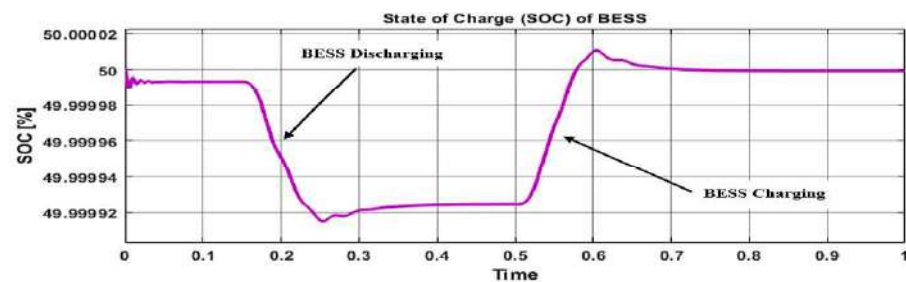
(a)



(b)



(c)

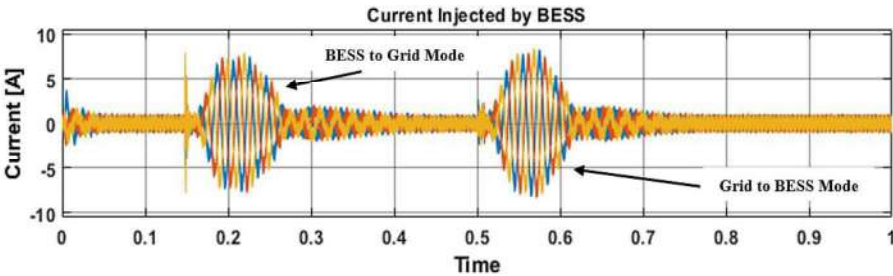


(d)

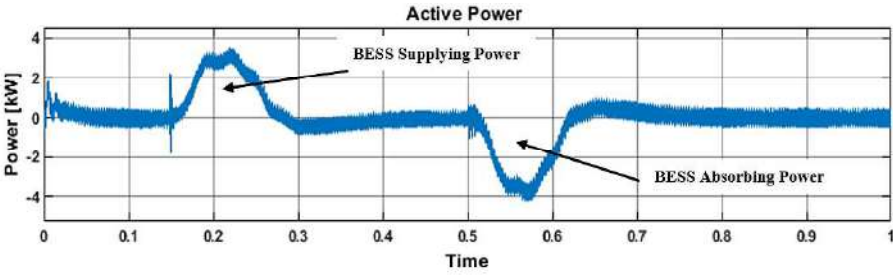
Fig. 5.4. Sudden load variation (a) DC link voltage (b) Adaptive current reference of BESS controller (c) BESS voltage and (d) State of charge (SOC) of BESS

Due to load variations in the system, the DC link voltage at the inverter side changes. The controller helps keep the DC link voltage steady, as shown in Fig. 5.4(a). BESS current reference is shown in Fig. 5.4(b) which is adaptive in nature whose value depends on the frequency deviation and ROCOF. The BESS remains in inactive condition when the grid frequency becomes equal to the nominal frequency (i.e. 50 Hz). Since the suggested

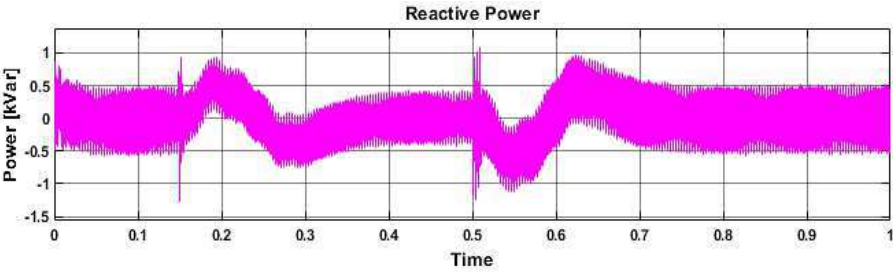
model does not support reactive power, the overload condition causes the voltage at PCC to fall. To reduce the complexity of the controller's design, the reference value for reactive power supply by BESS has been set to zero. Therefore, BESS provides zero reactive power on average. From Fig. 5.5(b), it is seen that, BESS is supplying active power to the grid for under-frequency condition of the grid whereas it absorbs active power from the grid during over-frequency event to provide necessary inertial support. The adaptive defuzzified value of the FLC system is also shown in Fig. 5.5(f) that confirms the instantaneous variation of current reference with the instantaneous value of frequency deviation and ROCOF.



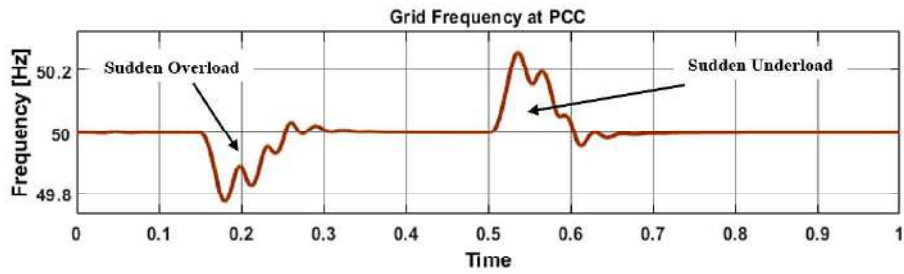
(a)



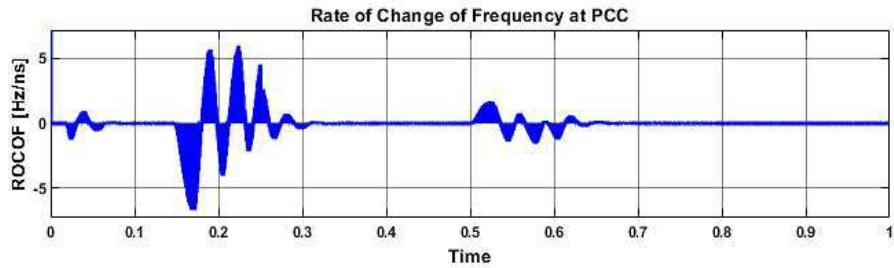
(b)



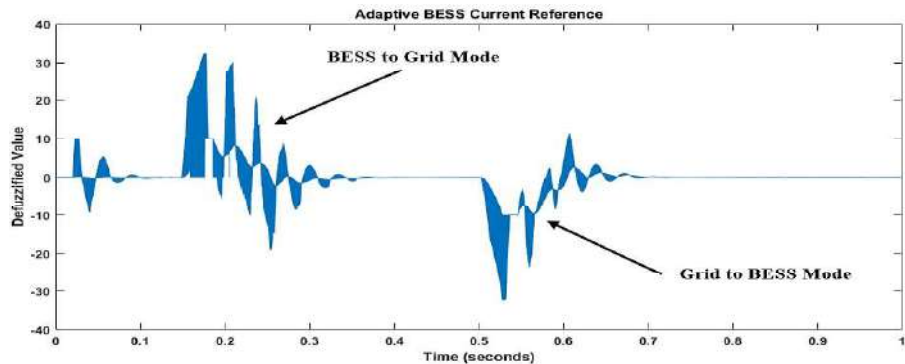
(c)



(d)



(e)



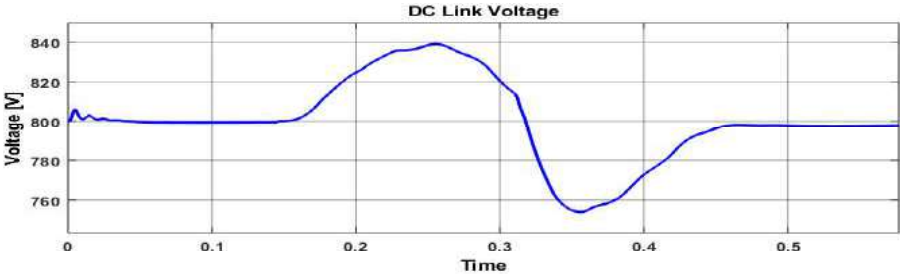
(f)

Fig. 5.5. Sudden load variation (a) Current injected by BESS (b) Active power supplied or absorbed by BESS (c) Reactive power supplied or absorbed by BESS (d) Grid frequency at PCC (e) Rate of change of frequency (ROCOF) and (f) Adaptive defuzzified value of FLC

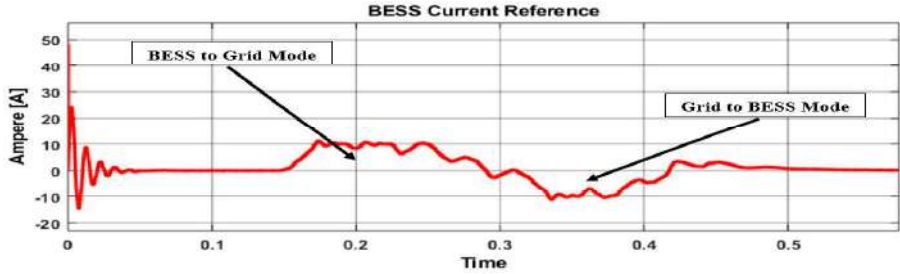
According to Fig. 5.5(d), sudden load injection causes a reduction in system frequency while sudden load rejection causes a rise in frequency. During the test, the frequency nadir and maximum frequency overshoot were found to be 49.773 Hz and 50.022 Hz respectively for sudden load injection and for sudden load rejection, the values were recorded to be 49.965 Hz and 50.284 Hz respectively. In comparison to load rejection, the ROCOF value for load injection was greater. The grid frequency stabilizes after 157 ms and 150 ms respectively the test cases.

5.3.2 Three phase dead short circuit fault at PCC

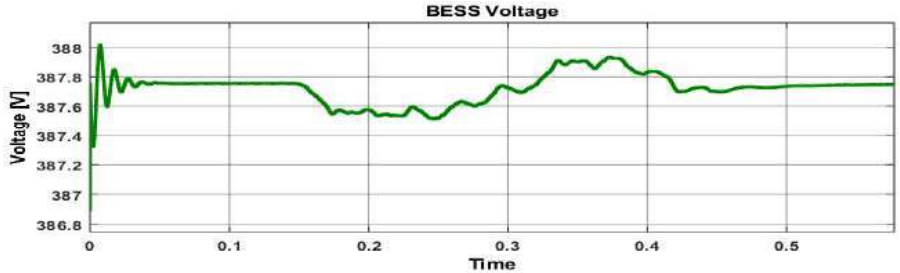
Similarly, a three-phase short circuit has been applied at PCC to see the effectiveness of the proposed controller under transient event. The fault has been applied at $t = 0.16$ s and withdrawn at $t = 0.31$ s.



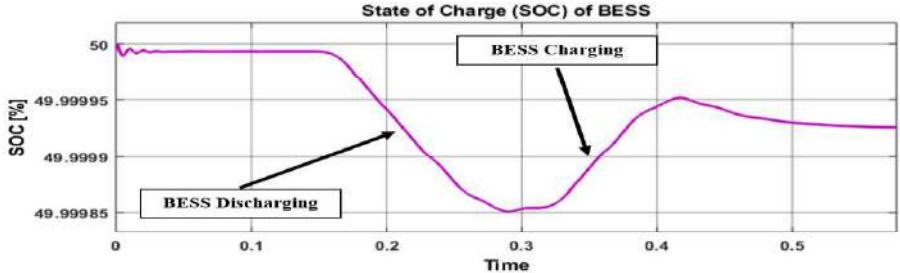
(a)



(b)



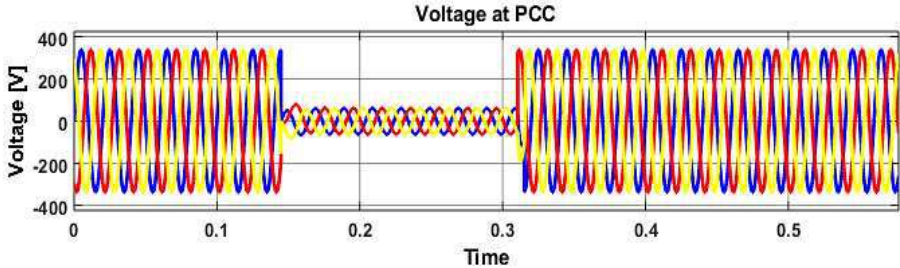
(c)



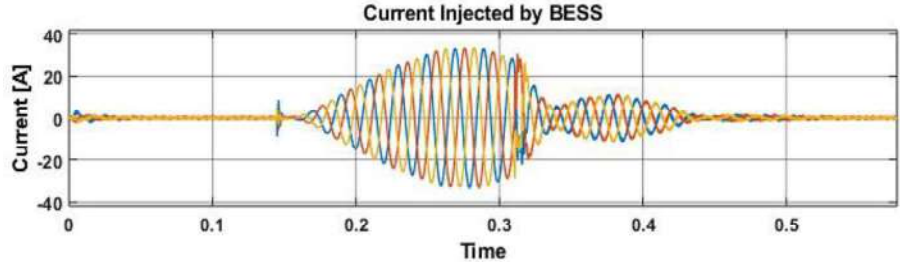
(d)

Fig. 5.6. Three phase short circuit fault at PCC (a) DC link voltage (b) Adaptive current reference of BESS controller (c) BESS voltage and (d) State of charge (SOC) of BESS

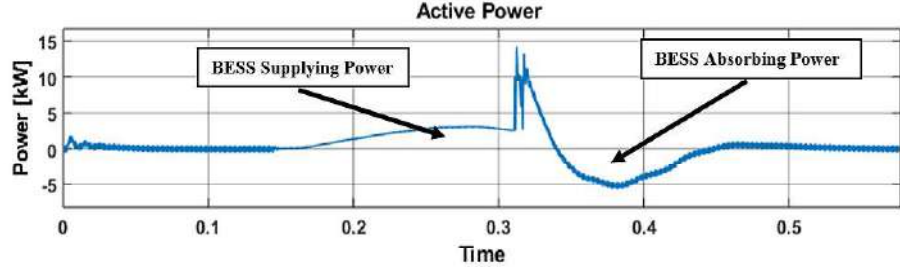
The frequency of the system varied significantly during the base case whereas, the variation in frequency has been found to be reduced due to the BESS action accompanied with the proposed adaptive controller. Fig. 5.6 shows the BESS parameters in response to the transient event. For this case also, the DC link voltage is regulated to 800 V and the current reference for BESS action varies adaptively to minimize the effect on frequency variations. The BESS SOC is shown in Fig. 5.6(d) that also confirms adaptive nature of the proposed controller.



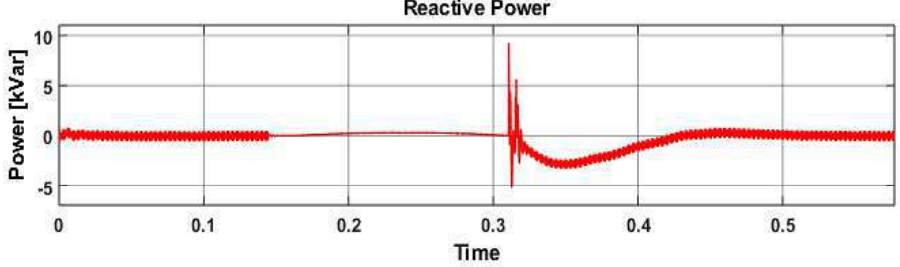
(a)



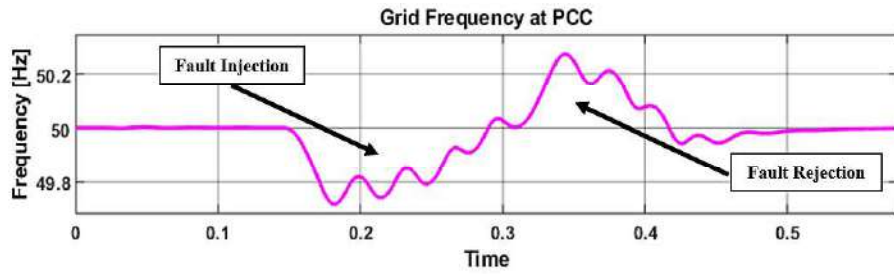
(b)



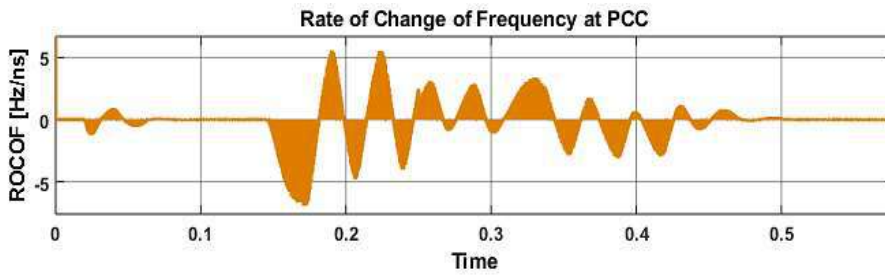
(c)



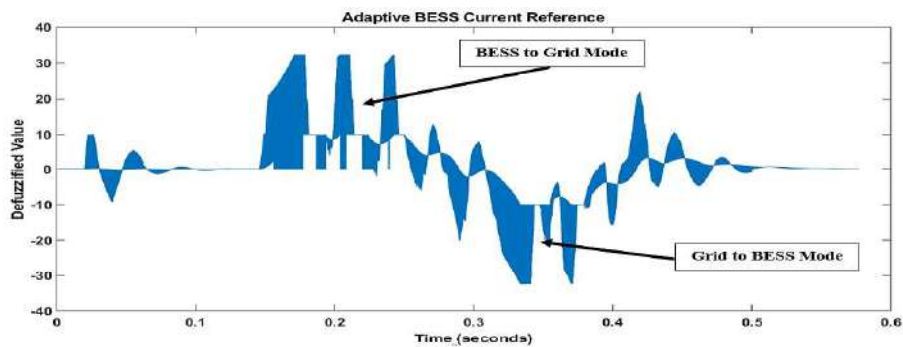
(d)



(e)



(f)



(g)

Fig. 5.7. Three phase short circuit fault at PCC (a) Voltage at PCC (b) Current injected by BESS (c) Active power supplied or absorbed by BESS (d) Reactive power supplied or absorbed by BESS (e) Grid frequency at PCC (f) Rate of change of frequency (ROCOF) and (g) Adaptive defuzzified value of FLC

The voltage at PCC becomes almost zero during the fault and the current injected by the BESS also increases to provide inertial support to the grid as shown in Fig. 5.7(b). When the system was subjected to the fault, frequency of the system falls and the minimum frequency of the system during this event was found to be 49.723 Hz. After the system stabilizes, the fault was withdrawn from the system. The maximum frequency recorded during this event was founded to be 50.311 Hz as seen from Fig. 5.7(e). The active power delivered/absorbed varies depending on the frequency variation and ROCOF of the grid as shown in Fig. 5.7(c). Although the reactive power to be supplied or absorbed by the

BESS should be zero, but certain amount of reactive power is being absorbed by BESS when fault is removed from the system as shown in Fig. 5.7(d). A significant reduction of ROCOF value has been observed for this case and the settling time required for the system to be stable was 210 ms for fault injection whereas for fault rejection, the settling time was only 165 ms.

5.4 Comparative Analysis

Table 5.1 shows the comparative analysis of the improvements as recorded by authors by utilizing the proposed controller with the base case i.e. with a BESS adopting fuzzy logic and PI controller. The recorded data shows that, a significant improvements of frequency nadir (i.e. minimum frequency, Hz) and ROCOF have been found by implementing the proposed hybrid BESS controller. During overload condition, the frequency nadir for base case was to be 49.556 Hz whereas after using the proposed controller, the frequency nadir was observed to be 49.773 Hz. Hence, an improvement by 0.43% in frequency nadir has been found for load injection. Similarly for three phase short circuit event, the frequency nadir was found to be 49.421 Hz for base case whereas the value was only 49.723 Hz for the proposed algorithm. For this case, the frequency nadir has been found to be improved by 0.61% than the base case. The replacement of PI controller by ANFIS model significantly improved the settling time required for the system to be stable after each disturbance as discussed previously in this section. Moreover, an improvement in ROCOF has been found for the proposed case than the base case as shown in the table.

Table 5.2 shows a comparison of this work with some relevant works done by the researchers. Although the system considered for analysis is different, but a comparison can be shown from the perspective of percentage improvement in rate of change of frequency (ROCOF) and frequency nadir. The study shows that, the controller proposed in this thesis work outperforms the controller designed by the authors as mentioned in the table. Hence, the designed controller can be used for improving inertia of a low inertia system.

Table 5.1: Comparative analysis between FLC-PI and FLC-ANFIS based BESS controller performance

Cases	BESS using Fuzzy logic and PI controller			BESS adopting Fuzzy-ANFIS hybrid controller			Remarks
	Maximum frequency (f_{max}) (Hz)	Minimum frequency (f_{nadir}) (Hz)	Maximum rate of change of frequency ($ROCOF_{max}$) (Hz/ns)	Maximum frequency (f_{max}) (Hz)	Minimum frequency (f_{nadir}) (Hz)	Maximum rate of change of frequency ($ROCOF_{max}$) (Hz/ns)	
Load injection	50.113	49.556	-13.50	50.022	49.773	-6.83	BESS with proposed controller outperforms from the perspective of f_{max} , f_{nadir} and $ROCOF_{max}$
Load rejection	50.512	49.863	+4.23	50.284	49.965	+1.92	
Fault injection	50.127	49.421	-14.21	50.033	49.723	-7.32	
Fault rejection	50.451	49.807	+5.51	50.311	49.967	+3.40	

Table 5.2: Comparison of the performance of FLC-ANFIS based BESS controller with related works

Paper Id	Methodology	System Frequency	Rate of change of frequency (ROCOF)	% Improvement in ROCOF	Frequency Nadir (Hz)	% Improvement in frequency nadir
[51]	BESS with FLC	50 Hz	-0.16 to -0.12	25%	49.84 to 49.88	0.08%
[52]	ANFIS	50 Hz	-	-	49.77 to 49.91	0.28%
[57]	Inverter Control	60 Hz	-13 to -8.5	34.61%	59.18 to 59.27	0.15%
			+12.5 to +7.5	40%		
This work	BESS with FLC & ANFIS	50 Hz	-13.5 to -6.8	49.63%	49.556 to 49.773	0.43%
			4.23 to 1.92	54.6%	49.863 to 49.965	0.20%
			-14.21 to -7.32	48.49%	49.421 to 49.723	0.61%
			5.51 to 3.40	38.29%	49.807 to 49.967	0.32%

5.5 Discussions

This chapter presents the design and implementation of the proposed BESS controller that can emulate virtual inertia by absorbing and releasing energy from/to the system based on the magnitude of frequency nadir and ROCOF. The adaptive nature of the controller helps to the improvement of system performance under abnormal scenarios. First of all, the controller was designed with the widely used PI controller and then due to having some limitations of the PI controller under transient event and non-adaptivity, ANFIS model has been utilized in place of PI controller to see the improvements in the frequency response under abnormal situations. Significant improvement in the frequency response has been observed as summarized in Table 5.1. The maximum frequency recorded during load rejection event was 50.512 Hz for FL-PI controller where it was recorded to be 50.284 Hz for FL-ANFIS.

Chapter-6

Conclusion and Future Works

6.1 Conclusion

An improved adaptive Fuzzy-ANFIS hybrid algorithm-based controller has been presented for a low inertia grid connected BESS application to provide frequency support emulating virtual inertia. An adaptive current reference for BESS controller is generated by the FLC-ANFIS hybrid controller based on the grid frequency and ROCOF. The elimination of the PI controller by using the ANFIS architecture enables the suggested controller to perform better in transient events. The suggested controller modifies the reference signal in accordance with the inputs to provide the required active power assistance for improving frequency stability and to give the grid a fictitious inertia similar to that of a traditional synchronous machine. The simulation results demonstrated that, in terms of frequency nadir and ROCOF, the suggested adaptive controller performs better than the base case. The given controller outperformed the PI-based controller in terms of frequency nadir by 0.43% for load injection and 0.20% for load rejection. Similarly, 0.61% improvement has been observed for transient short circuit fault injection and 0.32% for fault rejection. In addition to providing inertial assistance at the grid level, the suggested controller has a number of other uses. The suggested controller, in particular for microgrid applications, may perform superbly for simulating virtual inertia to improve grid stability and keep the frequency and ROCOF during dynamic grid scenarios within acceptable operating zone of IEEE 1547 standard. The provided controller can also be used for nanogrid applications to uphold system stability. The main limitation of the proposed model is the long-time taken by ANFIS model for training and the BESS not providing reactive power support for voltage stabilization.

6.2 Scope of the Future Works

Future work includes the following points-

- Inclusion of reactive power support in addition to the frequency support of the proposed controller.
- Application of machine learning algorithms for modelling the BESS controller.
- Implementation of optimization technique to identify BESS size.

References

- [1] Atte Harjanne, Janne M. Korhonen, Abandoning the concept of renewable energy, *Energy Policy*, Volume 127, 2019, Pages 330-340, ISSN 0301-4215, <https://doi.org/10.1016/j.enpol.2018.12.029>.
- [2] Ali Q. Al-Shetwi, M.A. Hannan, Ker Pin Jern, M. Mansur, T.M.I. Mahlia, Grid-connected renewable energy sources: Review of the recent integration requirements and control methods, *Journal of Cleaner Production*, Volume 253, 2020, 119831, ISSN 0959-6526, <https://doi.org/10.1016/j.jclepro.2019.119831>.
- [3] Simon Jenniches, Assessing the regional economic impacts of renewable energy sources – A literature review, *Renewable and Sustainable Energy Reviews*, Volume 93, 2018, Pages 35-51, ISSN 1364-0321, <https://doi.org/10.1016/j.rser.2018.05.008>.
- [4] Muhammad Kamran, Current status and future success of renewable energy in Pakistan, *Renewable and Sustainable Energy Reviews*, Volume 82, Part 1, 2018, Pages 609-617, ISSN 1364-0321, <https://doi.org/10.1016/j.rser.2017.09.049>.
- [5] Dolf Gielen, Francisco Boshell, Deger Saygin, Morgan D. Bazilian, Nicholas Wagner, Ricardo Gorini, The role of renewable energy in the global energy transformation, *Energy Strategy Reviews*, Volume 24, 2019, Pages 38-50, ISSN 2211-467X, <https://doi.org/10.1016/j.esr.2019.01.006>.
- [6] Taner Güney, Renewable energy, non-renewable energy and sustainable development, *International Journal of Sustainable Development & World Ecology*, 26:5, 2019, 389-397, DOI: 10.1080/13504509.2019.1595214.
- [7] Kenneth Hansen, Christian Breyer, Henrik Lund, Status and perspectives on 100% renewable energy systems, *Energy*, Volume 175, 2019, Pages 471-480, ISSN 0360-5442, <https://doi.org/10.1016/j.energy.2019.03.092>.
- [8] Gernaat, D.E.H.J., de Boer, H.S., Daioglou, V. et al. Climate change impacts on renewable energy supply. *Nat. Clim. Chang.* 11, 119–125 (2021). <https://doi.org/10.1038/s41558-020-00949-9>.
- [9] M. S. Alam, F. S. Al-Ismael, A. Salem and M. A. Abido, "High-Level Penetration of Renewable Energy Sources Into Grid Utility: Challenges and Solutions," in *IEEE Access*, vol. 8, pp. 190277-190299, 2020, doi: 10.1109/ACCESS.2020.3031481.
- [10] R. M. Elavarasan et al., "A Comprehensive Review on Renewable Energy Development, Challenges, and Policies of Leading Indian States With an International Perspective," in *IEEE Access*, vol. 8, pp. 74432-74457, 2020, doi: 10.1109/ACCESS.2020.2988011.
- [11] Fazıl Gökgöz, Mustafa Taylan Güvercin, Energy security and renewable energy efficiency in EU, *Renewable and Sustainable Energy Reviews*, Volume 96, 2018, Pages 226-239, ISSN 1364-0321, <https://doi.org/10.1016/j.rser.2018.07.046>.
- [12] Xiaofeng Xu, Zhifei Wei, Qiang Ji, Chenglong Wang, Guowei Gao, Global renewable energy development: Influencing factors, trend predictions and countermeasures, *Resources Policy*, Volume 63, 2019, 101470, ISSN 0301-4207, <https://doi.org/10.1016/j.resourpol.2019.101470>.
- [13] W. S. W. Abdullah, M. Osman, M. Z. A. Ab Kadir, and R. Verayiah, "The Potential and Status of Renewable Energy Development in Malaysia," *Energies*, vol. 12, no. 12, p. 2437, Jun. 2019, doi: 10.3390/en12122437.
- [14] Abubakar Kabir Aliyu, Babangida Modu, Chee Wei Tan, A review of renewable energy development in Africa: A focus in South Africa, Egypt and Nigeria, *Renewable and Sustainable Energy Reviews*, Volume 81, Part 2, 2018, Pages 2502-2518, ISSN 1364-0321, <https://doi.org/10.1016/j.rser.2017.06.055>.
- [15] Syed Abdul Rehman Khan, Zhang Yu, Amine Belhadi, Abbas Mardani, Investigating the effects of renewable energy on international trade and environmental quality, *Journal of*

- Environmental Management, Volume 272, 2020, 111089, ISSN 0301-4797, <https://doi.org/10.1016/j.jenvman.2020.111089>.
- [16] A. Crivellaro et al., "Beyond low-inertia systems: Massive integration of grid-forming power converters in transmission grids," 2020 IEEE Power & Energy Society General Meeting (PESGM), 2020, pp. 1-5, doi: 10.1109/PESGM41954.2020.9282031.
- [17] P. Du and W. Li, "Frequency Response Impact of Integration of HVDC Into a Low-Inertia AC Power Grid," in IEEE Transactions on Power Systems, vol. 36, no. 1, pp. 613-622, Jan. 2021, doi: 10.1109/TPWRS.2020.2990304.
- [18] P. Moriarty and D. Honnery, Global renewable energy resources and use in 2050. Elsevier Inc., 2018. doi: 10.1016/B978-0-12-814104-5.00006-5.
- [19] M. S. Alam, F. S. Al-Ismael, A. Salem and M. A. Abido, "High-Level Penetration of Renewable Energy Sources Into Grid Utility: Challenges and Solutions," in IEEE Access, vol. 8, pp. 190277-190299, 2020, doi: 10.1109/ACCESS.2020.3031481.
- [20] K. S. Ratnam, K. Palanisamy, and G. Yang. "Future low-inertia power systems: Requirements, issues, and solutions-A review." Renewable and Sustainable Energy Reviews 124 (2020): 109773, <https://doi.org/10.1016/j.rser.2020.109773>.
- [21] C. Yongning, L. Yan, W. Zhen, L. Zhen, L. Hongzhi and Z. Zhankui, "The Characteristics and Challenge on Large-Scale Renewable Energy Grid Integration," 2019 IEEE Innovative Smart Grid Technologies - Asia (ISGT Asia), 2019, pp. 1393-1398, doi: 10.1109/ISGT-Asia.2019.8881344.
- [22] R. Shah, N. Mithulananthan, R.C. Bansal, V.K. Ramachandaramurthy, A review of key power system stability challenges for large-scale PV integration, Renewable and Sustainable Energy Reviews, Volume 41, 2015, Pages 1423-1436, ISSN 1364-0321, <https://doi.org/10.1016/j.rser.2014.09.027>.
- [23] I. Ndiaye, E. Ahmed, C. Burns, J. Nickerson and M. Falls, "Impact of Distributed Solar PV Systems Operation on Residential Feeders Performance," 2018 IEEE/PES Transmission and Distribution Conference and Exposition (T&D), 2018, pp. 1-5, doi: 10.1109/TDC.2018.8440352.
- [24] G. Bhatt and S. Afflulla, "Analysis of large scale PV penetration impact on IEEE 39-Bus power system," 2017 IEEE 58th International Scientific Conference on Power and Electrical Engineering of Riga Technical University (RTU CON), 2017, pp. 1-6, doi: 10.1109/RTU CON.2017.8124840.
- [25] Simon R. Sinsel, Rhea L. Riemke, Volker H. Hoffmann, Challenges and solution technologies for the integration of variable renewable energy sources—a review, Renewable Energy, Volume 145, 2020, Pages 2271-2285, ISSN 0960-1481, <https://doi.org/10.1016/j.renene.2019.06.147>.
- [26] D. Nguyen and J. Kleissl, "Research on impacts of distributed versus centralized solar resource on distribution network using power system simulation and solar now-casting with sky imager," 2015 IEEE 42nd Photovoltaic Specialist Conference (PVSC), 2015, pp. 1-3, doi: 10.1109/PVSC.2015.7356208.
- [27] Q. Tran, M. Cong Pham, L. Parent and K. Sousa, "Integration of PV Systems into Grid: From Impact Analysis to Solutions," 2018 IEEE International Conference on Environment and Electrical Engineering and 2018 IEEE Industrial and Commercial Power Systems Europe (EEEIC / I&CPS Europe), 2018, pp. 1-6, doi: 10.1109/EEEIC.2018.8494400.
- [28] Qianjin Zhang, Mingxuan Mao, Guo Ke, Lin Zhou and Bao Xie, Stability problems of PV inverter in weak grid: a review, IET Power Electronics, Volume 13, 2020, Pages 2165-2174, ISSN 1755-4535, DOI: 10.1049/iet-pel.2019.1049.
- [29] Y. Khayat, M. Naderi, H. Bevrani and F. Blaabjerg, "Chapter 19 - Virtual inertia emulating in power electronic-based power systems", Control of Power Electronic Converters and Systems, Academic Press, 2021, Pages 541-560, ISBN 9780128194324, <https://doi.org/10.1016/B978-0-12-819432-4.00019-6>.

- [30] K. M. Cheema, "A comprehensive review of virtual synchronous generator", *International Journal of Electrical Power & Energy Systems*, Volume 120, 2020, 106006, ISSN 0142-0615, <https://doi.org/10.1016/j.ijepes.2020.106006>.
- [31] K. M. Cheema et al., "Virtual synchronous generator: Modifications, stability assessment and future applications," *Energy Reports*, vol. 8, pp. 1704–1717, 2022, doi: <https://doi.org/10.1016/j.egy.2021.12.064>.
- [32] A. Haldar, R. Khatua, A. Malkhandi, N. Senroy and S. Mishra, "Delay Based Virtual Inertia Emulation for a Grid Forming System," 2022 IEEE Power and Energy Conference at Illinois (PECI), 2022, pp. 1-6, doi: 10.1109/PECI54197.2022.9744046.
- [33] P. Liu, Y. Bi and C. Liu, "Data-Based Intelligent Frequency Control of VSG via Adaptive Virtual Inertia Emulation," in *IEEE Systems Journal*, vol. 16, no. 3, pp. 3917-3926, Sept. 2022, doi: 10.1109/JSYST.2021.3131866.
- [34] K. Y. Yap, C. R. Sarimuthu, and J. M. Y. Lim, "Virtual inertia-based inverters for mitigating frequency instability in grid-connected renewable energy system: A Review," *Appl. Sci.*, vol. 9, no. 24, 2019, doi: 10.3390/app9245300.
- [35] K. R. Vasudevan, V. K. Ramachandaramurthy, T. S. Babu, and A. Pouryekta, "Synchronverter: A Comprehensive Review of Modifications, Stability Assessment, Applications and Future Perspectives," *IEEE Access*, vol. 8, pp. 131565–131589, 2020, doi: 10.1109/ACCESS.2020.3010001.
- [36] Q. Peng, J. Fang, Y. Yang, T. Liu and F. Blaabjerg, "Maximum Virtual Inertia From DC-Link Capacitors Considering System Stability at Voltage Control Timescale," in *IEEE Journal on Emerging and Selected Topics in Circuits and Systems*, vol. 11, no. 1, pp. 79-89, March 2021, doi: 10.1109/JETCAS.2021.3049686.
- [37] R. Zhang, J. Fang and Y. Tang, "Inertia Emulation through Supercapacitor Energy Storage Systems," 2019 10th International Conference on Power Electronics and ECCE Asia (ICPE 2019 - ECCE Asia), 2019, pp. 1365-1370, doi: 10.23919/ICPE2019-ECCEAsia42246.2019.8796987.
- [38] S. Mahajan, and Y. P. Verma. "Performance of fast responding ultracapacitor energy storage for virtual inertia emulation control." *Energy Storage* (2022), pp. 346. <https://doi.org/10.1002/est2.346>.
- [39] L. Toma et al., "On the virtual inertia provision by BESS in low inertia power systems," 2018 IEEE International Energy Conference (ENERGYCON), 2018, pp. 1-6, doi: 10.1109/ENERGYCON.2018.8398755.
- [40] M. Kosmecki et al., "A methodology for provision of frequency stability in operation planning of low inertia power systems," *Energies*, vol. 14, no. 3, 2021, doi: 10.3390/en14030737.
- [41] S. S. Sami, M. Cheng, and J. Wu, "Modelling and control of multi-type grid-scale energy storage for power system frequency response," 2016 IEEE 8th Int. Power Electron. Motion Control Conf. IPEMC-ECCE Asia 2016, pp. 269–273, 2016, doi: 10.1109/IPEMC.2016.7512297.
- [42] R. Ciavarella et al., "Modeling of an Energy Hybrid System Integrating Several Storage Technologies: The DBS Technique in a Nanogrid Application," *Sustainability*, vol. 13, no. 3. 2021. doi: 10.3390/su13031170.
- [43] M. Nagaiah, K. C. Sekhar, "Analysis of fuzzy logic controller based bi-directional DC-DC converter for battery energy management in hybrid solar/wind micro grid system," 2020 *International Journal of Electrical and Computer Engineering (IJECE)*, Vol. 10, No. 3, pp. 2271-2284, ISSN: 2088-8708, DOI: 10.11591/ijece.v10i3.pp2271-2284.
- [44] M. Faisal, M. A. Hannan, P. J. Ker and M. N. Uddin, "Backtracking Search Algorithm Based Fuzzy Charging-Discharging Controller for Battery Storage System in Microgrid Applications," in *IEEE Access*, vol. 7, pp. 159357-159368, 2019, doi: 10.1109/ACCESS.2019.2951132.

- [45] H. ZHAO, Q. WU, C. WANG, L. CHENG, and C. N. RASMUSSEN, "Fuzzy logic based coordinated control of battery energy storage system and dispatchable distributed generation for microgrid," *J. Mod. Power Syst. Clean Energy*, vol. 3, no. 3, pp. 422–428, 2015, doi: 10.1007/s40565-015-0119-x.
- [46] N. Tephiruk, W. Kanokbannakorn, T. Kerdphol, Y. Mitani, and K. Hongesombut, "Fuzzy Logic Control of a Battery Energy Storage System for Stability Improvement in an Islanded Microgrid," *Sustainability*, vol. 10, no. 5, p. 1645, May 2018, doi: 10.3390/su10051645.
- [47] F. Asghar, M. Talha, and S. H. Kim, "Fuzzy logic-based intelligent frequency and voltage stability control system for standalone microgrid," *Int. Trans. Electr. Energy Syst.*, vol. 28, no. 4, pp. 1–14, 2018, doi: 10.1002/etep.2510.
- [48] A. Hussain, V.-H. Bui, and H.-M. Kim, "Fuzzy Logic-Based Operation of Battery Energy Storage Systems (BESSs) for Enhancing the Resiliency of Hybrid Microgrids," *Energies*, vol. 10, no. 3, p. 271, Feb. 2017, doi: 10.3390/en10030271.
- [49] L. Toma et al., "Fuzzy Logic based Battery Energy Storage System Control for Frequency Containment," 2021 12th International Symposium on Advanced Topics in Electrical Engineering (ATEE), 2021, pp. 1-6, doi: 10.1109/ATEE52255.2021.9425081.
- [50] R. S. Salles, G. C. S. Almeida, B. I. Lima Fuly, A. C. Z. de Souza and P. F. Ribeiro, "Fuzzy Logic-Based Controller for BESS and Load Management in a Microgrid Economic Operation," 2020 IEEE PES Transmission & Distribution Conference and Exhibition - Latin America (T&D LA), 2020, pp. 1-6, doi: 10.1109/TDLA47668.2020.9326102.
- [51] S. Zhang, Y. Mishra and M. Shahidehpour, "Fuzzy-Logic Based Frequency Controller for Wind Farms Augmented With Energy Storage Systems," in *IEEE Transactions on Power Systems*, vol. 31, no. 2, pp. 1595-1603, March 2016, doi: 10.1109/TPWRS.2015.2432113.
- [52] K. Akbar, K. Shahram and A. Hamdi, "Microgrid frequency control using the virtual inertia and ANFIS-based Controller," 2019 International Journal of Industrial Electronics, Control and Optimization, Volume 2 , Number 2; Page(s) 145-154.
- [53] S. M. Alhejaj and F. M. Gonzalez-Longatt, "Investigation on grid-scale BESS providing inertial response support," 2016 IEEE International Conference on Power System Technology (POWERCON), 2016, pp. 1-6, doi: 10.1109/POWERCON.2016.7754049.
- [54] R. K. Sarojini, K. Palanisamy, and E. De Tuglie, "A Fuzzy Logic-Based Emulated Inertia Control to a Supercapacitor System to Improve Inertia in a Low Inertia Grid with Renewables," *Energies*, vol. 15, no. 4, p. 1333, Feb. 2022, doi: 10.3390/en15041333.
- [55] S. Tang, H. Yang, R. Zhao and X. Geng, "Influence of battery energy storage system on steady state stability of power system," 2009 International Conference on Electrical Machines and Systems, 2009, pp. 1-4, doi: 10.1109/ICEMS.2009.5382739.
- [56] Y. Chen, Y. Zhao, G. Geng, Q. Jiang, W. Liu and L. Li, "Suppression Strategy of Ultra-Low Frequency Oscillation in Yunnan Power Grid with BESS," 2019 North American Power Symposium (NAPS), 2019, pp. 1-6, doi: 10.1109/NAPS46351.2019.9000236.
- [57] A. Karaki, M. B. Shadmand, H. Abu-Rub and S. Bayhan, "Virtual Inertia Emulation Inspired Predictive Control to Improve Frequency Stability in Power Electronics Dominated Grid," 2021 IEEE 12th International Symposium on Power Electronics for Distributed Generation Systems (PEDG), 2021, pp. 1-6, doi: 10.1109/PEDG51384.2021.9494245.
- [58] Q. Xu, T. Dragicevic, L. Xie and F. Blaabjerg, "Artificial Intelligence-Based Control Design for Reliable Virtual Synchronous Generators," in *IEEE Transactions on Power Electronics*, vol. 36, no. 8, pp. 9453-9464, Aug. 2021, doi: 10.1109/TPEL.2021.3050197.
- [59] M. Chen, D. Zhou and F. Blaabjerg, "Enhanced Transient Angle Stability Control of Grid-Forming Converter Based on Virtual Synchronous Generator," in *IEEE Transactions on Industrial Electronics*, vol. 69, no. 9, pp. 9133-9144, Sept. 2022, doi: 10.1109/TIE.2021.3114723.

- [60] O. Stanojev, U. Markovic, P. Aristidou and G. Hug, "Improving Stability of Low-Inertia Systems using Virtual Induction Machine Synchronization for Grid-Following Converters," in *IEEE Transactions on Power Systems*, 2022, doi: 10.1109/TPWRS.2022.3187789.
- [61] Dmitry Baimel, Implementation of DQ0 control methods in high power electronics devices for renewable energy sources, energy storage and FACTS, *Sustainable Energy, Grids and Networks*, Volume 18, 2019, 100218, ISSN 2352-4677, <https://doi.org/10.1016/j.segan.2019.100218>.
- [62] Y. Levron, J. Belikov, and D. Baimel, "A Tutorial on Dynamics and Control of Power Systems with Distributed and Renewable Energy Sources Based on the DQ0 Transformation," *Applied Sciences*, vol. 8, no. 9, p. 1661, Sep. 2018, doi: 10.3390/app8091661.
- [63] J. Rocabert, A. Luna, F. Blaabjerg and P. Rodríguez, "Control of Power Converters in AC Microgrids," in *IEEE Transactions on Power Electronics*, vol. 27, no. 11, pp. 4734-4749, Nov. 2012, doi: 10.1109/TPEL.2012.2199334.
- [64] D. Karaboga and E. Kaya, "Adaptive network based fuzzy inference system (ANFIS) training approaches: a comprehensive survey," *Artif. Intell. Rev.*, vol. 52, no. 4, pp. 2263–2293, 2019, doi: 10.1007/s10462-017-9610-2.
- [65] J. Meng, D. Stroe, M. Ricco, G. Luo and R. Teodorescu, "A Simplified Model-Based State-of-Charge Estimation Approach for Lithium-Ion Battery With Dynamic Linear Model," in *IEEE Transactions on Industrial Electronics*, vol. 66, no. 10, pp. 7717-7727, Oct. 2019, doi: 10.1109/TIE.2018.2880668.
- [66] Liu, K., Li, K., Peng, Q. et al. A brief review on key technologies in the battery management system of electric vehicles. *Front. Mech. Eng.* 14, 47–64 (2019). <https://doi.org/10.1007/s11465-018-0516-8>.
- [67] J. Meng, G. Luo, M. Ricco, M. Swierczynski, D.-I. Stroe, and R. Teodorescu, "Overview of Lithium-Ion Battery Modeling Methods for State-of-Charge Estimation in Electrical Vehicles," *Applied Sciences*, vol. 8, no. 5, p. 659, Apr. 2018, doi: 10.3390/app8050659.
- [68] W. Li et al., "Parameter sensitivity analysis of electrochemical model-based battery management systems for lithium-ion batteries," *Appl. Energy*, vol. 269, p. 115104, 2020, doi: <https://doi.org/10.1016/j.apenergy.2020.115104>.
- [69] D. N. T. How, M. A. Hannan, M. S. Hossain Lipu and P. J. Ker, "State of Charge Estimation for Lithium-Ion Batteries Using Model-Based and Data-Driven Methods: A Review," in *IEEE Access*, vol. 7, pp. 136116-136136, 2019, doi: 10.1109/ACCESS.2019.2942213.
- [70] C. H. Chen, F. B. Planella, K. O'Regan, D. Gasto, W. D. Widanage and E. Kendrick, "Development of Experimental Techniques for Parameterization of Multiscale Lithium-ion Battery Models," 2020 *J. Electrochem. Soc.* 167 080534.
- [71] S. Li, J. Li, H. He, and H. Wang, "Lithium-ion battery modeling based on Big Data", *Energy Procedia*, Volume 159, 2019, Pages 168-173, ISSN 1876-6102, <https://doi.org/10.1016/j.egypro.2018.12.046>.
- [72] A. R. Garg, X. Peng, M. L. P. Le, K. Pareek, and C. M. M. Chin, "Design and analysis of capacity models for Lithium-ion battery," *Measurement*, vol. 120, pp. 114–120, 2018.
- [73] P. Shrivastava, T. K. Soon, M. Y. I. Bin Idris, and S. Mekhilef, "Overview of model-based online state-of-charge estimation using Kalman filter family for lithium-ion batteries," *Renew. Sustain. Energy Rev.*, vol. 113, p. 109233, 2019, doi: <https://doi.org/10.1016/j.rser.2019.06.040>.
- [74] S. A. Gorji, H. G. Sahebi, M. Ektesabi and A. B. Rad, "Topologies and Control Schemes of Bidirectional DC–DC Power Converters: An Overview," in *IEEE Access*, vol. 7, pp. 117997-118019, 2019, doi: 10.1109/ACCESS.2019.2937239.